
Non-Myopic Active Feature Acquisition via Pathwise Policy Gradients

Linus Aronsson
Department of Computer Science and
Engineering
Chalmers University of Technology &
University of Gothenburg
Gothenburg, Sweden
linaro@chalmers.se

Morteza Haghiri Chehreghani
Department of Computer Science and
Engineering
Chalmers University of Technology &
University of Gothenburg
Gothenburg, Sweden
morteza.chehreghani@chalmers.se

Abstract

Active feature acquisition (AFA) considers prediction problems in which features are costly to obtain and the learner adaptively decides which feature values to acquire for each instance and when to stop and predict. AFA can be formulated as a partially observable Markov decision process (POMDP), which naturally admits a sequential decision-making perspective. In this paper, we present *non-myopic pathwise policy gradients* (NM-PPG), a new AFA method built around this formulation. We introduce a continuous relaxation of the acquisition process that enables pathwise gradients through the full acquisition trajectory, avoiding the high variance of standard score-function policy gradients while allowing end-to-end optimization of a non-myopic acquisition policy. To better align training with deployment, we further develop a straight-through rollout scheme that follows hard feature acquisitions in the forward pass while backpropagating through the corresponding soft relaxation in the backward pass. We stabilize optimization with entropy regularization and staged temperature sharpening. Experiments on both synthetic and real-world datasets demonstrate that NM-PPG yields superior performance relative to state-of-the-art AFA baselines.

1 Introduction

Many predictive systems rely on features that are expensive, slow, invasive, or privacy sensitive to obtain. In medical decision support, ordering all tests for every patient may be costly and burdensome, and can delay treatment [1]. In recommender systems and personalized services, collecting many behavioral signals raises both monetary and privacy costs [2]. In interactive troubleshooting, each diagnostic query consumes time and user effort [3, 4]. Similar constraints also arise in robotics and sensor systems, where measurements require energy, time, or motion [5–7]. Related ideas have also recently appeared in LLM-based decision-making, where the model may strategically gather additional information in a cost-sensitive way at test time rather than answering immediately [8]. These settings motivate *active feature acquisition* (AFA), where a learner sequentially decides which feature values to acquire for each data instance, and when to stop and predict, so as to balance predictive quality against feature acquisition cost [9, 10].

AFA differs fundamentally from standard static feature selection, where a single subset of features is selected and used for all instances [11]. This can be suboptimal when the informative features vary across instances. For example, a cheap feature may reveal which one of several expensive features is actually relevant for the current instance. A static selector must typically retain all potentially relevant features in order to remain accurate across the population, whereas an *adaptive* AFA policy can first acquire the cheap indicator and then query only the appropriate expensive feature for that

particular instance [12]. In this sense, AFA can achieve a strictly better accuracy-cost trade-off than static selection by tailoring acquisition to the realized feature values of each instance.

AFA can be formulated as a *partially observable Markov decision process* (POMDP) [13]. A recent survey on AFA categorizes existing AFA methods around this POMDP formulation [10], such that the resulting taxonomy closely mirrors standard categorizations in the POMDP literature [13–15]. The survey identifies the following AFA categories. (i) Model-based methods, which estimate a model of the acquisition dynamics (i.e., a probability distribution over unobserved features given the already observed features) and learn an acquisition policy based on this [16–19]. (ii) Model-free methods, which avoid explicit modeling of the acquisition dynamics and instead learn acquisition policies directly from experience, either through oracle-guided supervision or reinforcement learning (RL) [9, 20–24]. Our method belongs to this category. (iii) Hybrid methods, which combine policy learning from experience with a learned model to improve supervision, state representations, or training stability [12, 25–28].

Our contributions are as follows:

- (i) We introduce a continuous relaxation of the AFA acquisition process that enables pathwise gradients through the entire acquisition trajectory (see Section 3.2). Prior non-myopic AFA methods face two complementary limitations. RL-based methods directly target long-term cost minimization in the AFA-POMDP, but rely on generic value-based or score-function RL methods such as DQN and PPO [21, 26, 29, 30], which are known to be highly unstable due to the intractability of AFA [12, 22, 24, 31]. Non-RL non-myopic methods instead exploit the structure of AFA to construct policies from jointly informative feature groups [12, 32], but this makes them biased relative to adaptive long-term cost minimization in the full AFA-POMDP; see Section 4.1 for details. Our method addresses both limitations by targeting long-term cost minimization while exploiting the structure of AFA through an AFA-specific continuous relaxation rather than generic RL. While continuous relaxations have been considered in prior AFA work [22–24, 33], these methods are fundamentally *myopic* in the sense that they optimize a one-step truncated approximation of the optimal value function, so gradients propagate only through a single acquisition step rather than through the full trajectory (see Appendices C.1 and G for details). In contrast, our method targets long-term cost minimization in the AFA-POMDP, naturally handles non-uniform feature costs, and yields a more principled treatment of the stopping decision, which myopic methods typically handle heuristically, for example by stopping once label confidence exceeds a threshold.
- (ii) We address the relaxation gap between the continuous relaxation and the underlying discrete acquisition process by introducing a straight-through rollout scheme, which follows hard feature acquisitions in the forward pass while backpropagating through the corresponding soft relaxation (see Section 3.3). This yields better alignment between training and the discrete test-time AFA process.
- (iii) We stabilize this pathwise objective using entropy regularization and staged temperature sharpening, providing a practical alternative to high-variance score-function policy gradients (see Section 3.4).
- (iv) Finally, we show experimentally that our method yields more stable performance than existing non-myopic AFA methods, outperforms myopic methods on datasets with non-myopic structure, and remains consistent with myopic baselines on datasets where myopic acquisition is sufficient (see Section 4.1).

2 Problem Formulation and Notation

Let $p(\mathbf{x}, \mathbf{y})$ be the data distribution, where $\mathbf{x} = (\mathbf{x}_1, \dots, \mathbf{x}_d) \in \mathcal{X}$ and $\mathbf{y} \in \mathcal{Y}$, with d denoting the number of features of each instance. Following most prior work on AFA, we focus on *classification* tasks in this paper, so the label space \mathcal{Y} is assumed to be a finite set of class labels. Nevertheless, the proposed method extends straightforwardly to regression tasks as well. Random variables are denoted by bold symbols (e.g. \mathbf{x}, \mathbf{y}), while their realizations are written in regular font, that is, $x, y \sim p(\mathbf{x}, \mathbf{y})$. For an instance $x \in \mathcal{X}$, acquiring feature $a \in [d] \triangleq \{1, \dots, d\}$ incurs a cost $c(a) \in \mathbb{R}^+$. For any subset $A \subseteq [d]$, we let $x_A \triangleq \{x_a \mid a \in A\}$ denote the subvector of x indexed by A . Similarly, for a random vector \mathbf{x} , we write \mathbf{x}_A for the corresponding random subvector. For any subsets $A, B \subseteq [d]$,

we write $p(\mathbf{x}_A, \mathbf{y} \mid x_B)$ for the conditional distribution under the true data distribution. For any finite set \mathcal{A} , let $\Delta(\mathcal{A}) \triangleq \{p \in \mathbb{R}^{|\mathcal{A}|} \mid p_i \geq 0 \text{ for all } i, \sum_{i=1}^{|\mathcal{A}|} p_i = 1\}$ denote the probability simplex over \mathcal{A} , that is, the set of all discrete probability distributions over the elements of \mathcal{A} .

AFA Procedure and Predictor with Partially Observed Inputs. For an instance $x \in \mathcal{X}$, features are acquired *adaptively* over a number of selection steps by a parameterized policy π_θ . A common way to represent partially observed inputs in AFA is via feature masking [10]. At selection step $0 \leq t \leq k$, let $m_t \in \{0, 1\}^d$ denote the current observation mask, where $m_{t,a} = 1$ if feature $a \in [d]$ has been observed by step t , and $m_{t,a} = 0$ otherwise. We assume $m_0 \in \{0\}^d$ (no observed features initially). We denote the corresponding sets of observed and unobserved feature indices at step t by $S_t \triangleq \{a \in [d] \mid m_{t,a} = 1\}$ and $U_t \triangleq [d] \setminus S_t$. Let \odot denote elementwise multiplication. We then represent the currently observed features and the action space by

$$x(m_t) \triangleq (m_t \odot x, m_t) \in \mathbb{R}^{2d}, \quad \mathcal{A} = \{1, \dots, d, d+1\}. \quad (1)$$

Here, $m_t \odot x \in \mathbb{R}^d$ is the masked feature vector, in which observed features retain their true values and unobserved features are set to zero, while the mask m_t itself is concatenated to indicate which features have been observed. Given the currently observed features, represented by $x(m_t)$, the policy outputs a probability distribution over the available actions. The policy is therefore defined as $\pi_\theta : \mathcal{X} \times \{0, 1\}^d \rightarrow \Delta(\mathcal{A})$, and $\pi_\theta(\cdot \mid x(m_t)) \in \Delta(\mathcal{A})$. Thus, $\pi_\theta(a \mid x(m_t))$ denotes the probability of selecting action $a \in \mathcal{A}$ given the currently observed features. At step $t < k$, an action $a_t \in \mathcal{A}$ is selected by sampling $a_t \sim \pi_\theta(\cdot \mid x(m_t))$. If $a_t \in [d]$, the cost $c(a_t)$ is incurred and feature x_{a_t} is acquired. The mask is then updated as $m_{t+1} = m_t + (1 - m_t) \odot \text{onehot}(a_t)$, where $\text{onehot}(a_t) \in \{0, 1\}^d$ denotes a one-hot vector where the a_t -th entry is 1 and remaining entries are 0. If $a_t = d+1$, the acquisition process terminates, and a prediction of the label is made given $x(m_t)$ (the predictor is defined below). Since the AFA problem is known to be highly intractable [10], we follow much prior AFA work and consider a fixed truncation horizon $k \leq d$: if the stop action has not been selected before step k , we force stopping at step k (i.e., $a_k = d+1$). In practice, a feature may not be acquired more than once, so for any $a \in S_t$, we force $\pi_\theta(a \mid x(m_t)) = 0$. In AFA, the predictor (similar to the policy) must operate on partially observed inputs. Using the masked representation introduced above, for any observation mask $m_t \in \{0, 1\}^d$, the predictor takes as input $x(m_t) \in \mathbb{R}^{2d}$ and outputs a probability distribution over the class labels in \mathcal{Y} . The predictor is therefore defined as $f_\phi : \mathcal{X} \times \{0, 1\}^d \rightarrow \Delta(\mathcal{Y})$, and $f_\phi(x(m_t)) \in \Delta(\mathcal{Y})$. Concretely, $f_\phi(x(m_t))$ is intended to approximate the Bayes optimal conditional predictive distribution $p(\mathbf{y} \mid x_{S_t})$.

Optimization Objective. Let $t_\theta(x) \leq k$ denote the stopping step for instance x under policy π_θ . Also, let $c(m_t) \triangleq \sum_{a \in [d]} m_{t,a} c(a)$ denote the total acquisition cost incurred up to step t . A standard optimization objective in the AFA literature is to minimize the expected prediction loss and feature acquisition cost across instances [10]:

$$\min_{\theta} \mathbb{E}_{\mathbf{x}, \mathbf{y}} \mathbb{E}_{\pi_\theta} [\ell(f_\phi(\mathbf{x}(m_{t_\theta}(\mathbf{x}))), \mathbf{y}) + \alpha c(m_{t_\theta}(\mathbf{x}))], \quad (2)$$

where $\phi \triangleq \arg \min_{\phi'} \mathbb{E}_{\mathbf{x}, \mathbf{y}, \mathbf{m}} [\ell(f_{\phi'}(\mathbf{x}(\mathbf{m})), \mathbf{y})]$ with $\mathbf{m} \sim \text{Uniform}(\{0, 1\}^d)$. Also, ℓ is a prediction loss and $\alpha \geq 0$ trades off prediction loss and acquisition cost. Following the vast majority of prior work on AFA, we consider the *offline* setting [10], where we assume access to a fully observed training dataset $\{(x^{(1)}, y^{(1)}), \dots, (x^{(n)}, y^{(n)})\} \sim p(\mathbf{x}, \mathbf{y})$. This dataset is then used to learn and evaluate the predictor f_ϕ and policy π_θ .

3 Proposed Method

In this section, we describe our proposed method.

3.1 AFA-POMDP Instantiation for the Standard Objective

The acquisition process in AFA (see Section 2) can be formulated as a finite-horizon POMDP [10, 34]. A formal definition of the AFA-POMDP is deferred to Appendix F. A state is represented by $(m_t, x, y) \in \{0, 1\}^d \times \mathcal{X} \times \mathcal{Y}$, where m_t is the current observation mask, while the agent observes only $x(m_t)$ and chooses actions $a_t \in \mathcal{A}$ as defined in (1). If $a_t \in [d]$, the state transitions to the updated mask m_{t+1} , which includes the newly acquired feature as described in Section 2. Let $C((m_t, x, y), a_t)$

denote the immediate cost of taking action a_t in state (m_t, x, y) . We set $C((m_t, x, y), a) = \alpha c(a)$ for feature acquisitions $a \in [d]$, while for stopping, $C((m_t, x, y), d+1) = \ell(f_\phi(x(m_t)), y)$. Let $\ell_t \triangleq \ell(f_\phi(x(m_t)), y)$, and recall that $t_\theta(x)$ denotes the stopping step for instance x under policy π_θ . For an instance $(x, y) \sim p(\mathbf{x}, \mathbf{y})$, with actions sampled as $a_t \sim \pi_\theta(\cdot | x(m_t))$, the trajectory cost $G(x, y, \pi_\theta)$ and expected cost $J(\pi_\theta)$ are

$$G(x, y, \pi_\theta) \triangleq \sum_{t=0}^{t_\theta(x)} C((m_t, x, y), a_t) = \sum_{t=0}^{t_\theta(x)-1} \alpha c(a_t) + \ell_{t_\theta(x)}, \quad J(\pi_\theta) \triangleq \mathbb{E}_{\mathbf{x}, \mathbf{y}, \pi_\theta} [G(\mathbf{x}, \mathbf{y}, \pi_\theta)]. \quad (3)$$

As in Section 2, we force stopping after $k \leq d$ steps. The following theorem states that minimizing expected cost in this POMDP is equivalent to optimizing the standard AFA objective in (2).

Theorem 1 [9]. *Minimizing $J(\pi_\theta)$ in (3) is equivalent to the optimization problem in (2).*

All proofs are provided in Appendix A. A standard way to optimize $J(\pi_\theta)$ in RL is via the *policy gradient theorem* (PGT) [35], which expresses the gradient $\nabla_\theta J(\pi_\theta)$ using the score function $\nabla_\theta \log \pi_\theta(a_t | x(m_t))$. We formally define the PGT w.r.t. (3) in Appendix F. The PGT provides an unbiased estimator of $\nabla_\theta J(\pi_\theta)$ even for discrete actions and non-differentiable trajectories, since it does not require differentiating through sampled actions or state transitions. However, score-function estimators often suffer from high variance, making optimization difficult and typically requiring variance-reduction techniques [23, 36, 37]. This approach is also common in prior AFA work, where π_θ is optimized with standard RL methods that utilize the PGT, such as PPO [26]. In this work, we propose an alternative method that enables direct pathwise gradients through a continuous relaxation of the AFA problem, which we introduce in the next subsection.

3.2 Pathwise Policy Gradients via a Differentiable Relaxation of the AFA-POMDP

Since the acquisition actions in AFA are discrete, pathwise gradients are not directly available. To address this, we replace the hard observation mask $m_t \in \{0, 1\}^d$ by a soft mask $\tilde{m}_t \in [0, 1]^d$, where $\tilde{m}_{t,j}$ represents the degree to which feature j has been acquired by step t . At step t , a neural network parameterized by θ outputs logits $z_t \triangleq z_\theta(x(\tilde{m}_t)) \in \mathbb{R}^{d+1}$, where $z_{t,1:d}$ are the feature-acquisition logits and $z_{t,d+1}$ is the stop logit; we use analogous indexing notation below for other action-indexed quantities. The corresponding policy is $\pi_\theta(\cdot | x(\tilde{m}_t)) = \text{softmax}(z_t/\tau_{\text{hard}})$, where $\tau_{\text{hard}} > 0$. To obtain a differentiable sample from this policy, we use the Gumbel-Softmax reparameterization [38, 39]:

$$\tilde{a}_t = \text{softmax}((z_t/\tau_{\text{hard}} + \varepsilon_t)/\tau_{\text{soft}}) \in [0, 1]^{d+1}, \quad \varepsilon_t \sim \text{Gumbel}(0, 1)^{d+1}. \quad (4)$$

The relaxed feature-acquisition distribution conditioned on not stopping is therefore

$$\tilde{r}_t = \text{softmax}((z_{t,1:d}/\tau_{\text{hard}} + \varepsilon_{t,1:d})/\tau_{\text{soft}}) \in [0, 1]^d. \quad (5)$$

For finite $\tau_{\text{soft}} > 0$, $1 - \tilde{a}_{t,d+1} > 0$, and $\tilde{r}_t = \tilde{a}_{t,1:d}/(1 - \tilde{a}_{t,d+1})$. Thus, \tilde{r}_t can be interpreted as the relaxed feature-acquisition distribution conditioned on not stopping. The corresponding hard feature action is sampled from the feature distribution conditioned on not stopping:

$$r_t = \text{onehot}(\text{argmax}_{j \in [d]}(\tilde{r}_{t,j})) \in \{0, 1\}^d. \quad (6)$$

By the Gumbel-Softmax reparameterization, obtaining the hard action in (6) is equivalent to sampling $r_t \sim \text{softmax}(z_{t,1:d}/\tau_{\text{hard}})$; see Appendix D. To match the discrete AFA process, if $r_{t,j} = 1$, feature j is treated as acquired and made unavailable in later steps by setting $z_{t',j} = -\infty$ for all $t' > t$. We also introduce a relaxed survival mass $\tilde{s}_t \in [0, 1]$, which represents the amount of relaxed mass that remains active at step t . The relaxed acquisition process then evolves according to

$$\tilde{m}_{t+1} = \tilde{m}_t + (1 - \tilde{m}_t) \odot \tilde{r}_t, \quad \tilde{s}_{t+1} = \tilde{s}_t(1 - \tilde{a}_{t,d+1}) = \prod_{i=0}^t (1 - \tilde{a}_{i,d+1}), \quad (7)$$

where $t = 0, \dots, k-1$ and $\tilde{s}_0 = 1$. The updated mask \tilde{m}_{t+1} describes the mass that continues after step t , and is therefore updated using \tilde{r}_t . Let $\tilde{\ell}_t \triangleq \ell(f_\phi(x(\tilde{m}_t)), y)$ and $c(\tilde{r}_t) \triangleq \sum_{j=1}^d \tilde{r}_{t,j} c(j)$. The relaxed trajectory cost $\tilde{G}(x, y, \theta, \varepsilon)$ and corresponding objective $\tilde{J}(\theta)$ are then

$$\tilde{G}(x, y, \theta, \varepsilon) \triangleq \sum_{t=0}^{k-1} \tilde{s}_t (\alpha(1 - \tilde{a}_{t,d+1})c(\tilde{r}_t) + \tilde{a}_{t,d+1}\tilde{\ell}_t) + \tilde{s}_k \tilde{\ell}_k, \quad \tilde{J}(\theta) \triangleq \mathbb{E}_{\mathbf{x}, \mathbf{y}} \mathbb{E}_\varepsilon [\tilde{G}(\mathbf{x}, \mathbf{y}, \theta, \varepsilon)]. \quad (8)$$

Here, \tilde{s}_t is the survival mass that reaches step t . A fraction $\tilde{a}_{t,d+1}$ of this mass stops and incurs prediction loss, while the remaining fraction $1 - \tilde{a}_{t,d+1}$ continues after acquiring a feature according to \tilde{r}_t . In this sense, the finite-temperature process is a differentiable soft-branching relaxation of the discrete AFA dynamics. See Appendix D for details. The final term $\tilde{s}_k \tilde{\ell}_k$ represents forced terminal prediction at step k , which matches the discrete problem defined in Section 2. Moreover, the following theorem provides important properties of the relaxation:

Theorem 2. *The following claims hold for the continuous relaxation of the AFA-POMDP in (8): (i) $\tilde{m}_t \in [0, 1]^d$ for all t ; (ii) the induced relaxed stopping weights form a normalized distribution over stopping steps, i.e. $\sum_{t=0}^{k-1} \tilde{s}_t \tilde{a}_{t,d+1} + \tilde{s}_k = 1$ for any k ; (iii) if each \tilde{a}_t is hard, that is, $\tilde{a}_t \in \{0, 1\}^{d+1}$ for all t , then the relaxed trajectory cost in (8) equals the discrete trajectory cost in (3); and (iv) as $\tau_{\text{soft}} \rightarrow 0$, the actions \tilde{a}_t become hard almost surely over the Gumbel noise.*

Property (ii) of Theorem 2 makes the loss terms in (8) a natural soft analogue of the terminal loss in the discrete AFA process. Although the relaxed process evaluates the prediction loss at every step, the loss at step t is weighted by the relaxed mass assigned to stopping at that step, $\tilde{s}_t \tilde{a}_{t,d+1}$, with the remaining survival mass assigned to forced stopping at k . Thus, the relaxation defines a normalized soft weighting over stopping steps. Overall, the relaxed formulation preserves the branching structure of the discrete problem while providing a natural differentiable surrogate for optimization, and properties (iii) and (iv) of Theorem 2 suggest annealing τ_{soft} toward zero during training to gradually align the relaxed trajectory cost with the corresponding discrete cost. See Appendix D for details about the continuous relaxation. Because the relaxed AFA formulation has continuous actions and a deterministic policy via the reparameterization in (4), the *deterministic policy gradient* (DPG) theorem [37, 40, 41] can be used. We define the DPG theorem for the relaxed AFA formulation in Appendix F.3. However, our relaxed problem yields another alternative due to additional structure in the relaxation. Beyond (4), the relaxed state dynamics in (7) and the relaxed trajectory cost in (8) are both differentiable. Therefore, the relaxed rollout defines a differentiable computation graph with respect to θ . As a result, the relaxed objective in (8) can be optimized directly by differentiating through the entire trajectory, i.e., $\nabla_{\theta} \tilde{J}(\theta) = \mathbb{E}_{\mathbf{x}, \mathbf{y}} \mathbb{E}_{\varepsilon} [\nabla_{\theta} \tilde{G}(\mathbf{x}, \mathbf{y}, \theta, \varepsilon)]$.

3.3 Reducing the Relaxation Gap via Straight-Through Rollouts

The objective in (8) is optimized under a continuous process, while at inference we operate on the discrete AFA process in (3). To reduce this gap, we use a straight-through (ST) rollout [38, 42]. At step t , let \tilde{r}_t be the conditional feature-acquisition distribution and r_t the corresponding hard feature action from Section 3.2. We construct ST variables for the conditional feature action and mask:

$$\bar{r}_t = r_t - \text{sg}(\tilde{r}_t) + \tilde{r}_t, \quad \bar{m}_{t+1} = m_{t+1} - \text{sg}(\tilde{m}_{t+1}) + \tilde{m}_{t+1}. \quad (9)$$

Here, $\text{sg}(\cdot)$ denotes stop-gradient, i.e., $\text{sg}(u) = u$ and $\partial \text{sg}(u) / \partial u = 0$. The hard mask follows $m_{t+1} = m_t + (1 - m_t) \odot r_t$, while the relaxed mask follows (7). Consequently, in the forward pass, $\bar{r}_t = r_t$ and $\bar{m}_t = m_t$, so the predictor and policy are evaluated on hard masks. In the backward pass, gradients pass through the relaxed variables, since $\partial \bar{r}_t / \partial \tilde{r}_t = I$ and $\partial \bar{m}_t / \partial \tilde{m}_t = I$. Let $\bar{\ell}_t \triangleq \ell(f_{\phi}(x(\bar{m}_t)), y)$. We define the ST trajectory objective as

$$\bar{G}(x, y, \theta, \varepsilon) \triangleq \sum_{t=0}^{k-1} \tilde{s}_t (\alpha(1 - \tilde{a}_{t,d+1}) c(\bar{r}_t) + \tilde{a}_{t,d+1} \bar{\ell}_t) + \tilde{s}_k \bar{\ell}_k, \quad \bar{J}(\theta) \triangleq \mathbb{E}_{\mathbf{x}, \mathbf{y}} \mathbb{E}_{\varepsilon} [\bar{G}(\mathbf{x}, \mathbf{y}, \theta, \varepsilon)]. \quad (10)$$

Because \bar{r}_t and \bar{m}_t use stop-gradient operations, automatic differentiation gives a straight-through surrogate gradient rather than the exact derivative of the hard-forward objective. We write this estimator as $\nabla_{\theta}^{\text{ST}} \bar{J}(\theta) \triangleq \mathbb{E}_{\mathbf{x}, \mathbf{y}} \mathbb{E}_{\varepsilon} [\nabla_{\theta}^{\text{ST}} \bar{G}(\mathbf{x}, \mathbf{y}, \theta, \varepsilon)]$. The following proposition gives $\nabla_{\theta}^{\text{ST}} \bar{G}$ for a fixed rollout.

Proposition 1. *For a fixed rollout (x, y, ε) , the ST surrogate gradient of \bar{G} in (10) expands as*

$$\nabla_{\theta}^{\text{ST}} \bar{G}(x, y, \theta, \varepsilon) = \sum_{t=0}^k \left(\frac{\partial \bar{G}}{\partial \bar{r}_t} \frac{\partial \bar{r}_t}{\partial \tilde{r}_t} \frac{\partial \tilde{r}_t}{\partial \theta} + \frac{\partial \bar{G}}{\partial \tilde{a}_{t,d+1}} \frac{\partial \tilde{a}_{t,d+1}}{\partial \theta} + \frac{\partial \bar{G}}{\partial \bar{m}_t} \frac{\partial \bar{m}_t}{\partial \tilde{m}_t} \frac{\partial \tilde{m}_t}{\partial \theta} + \frac{\partial \bar{G}}{\partial \tilde{s}_t} \frac{\partial \tilde{s}_t}{\partial \theta} \right). \quad (11)$$

Here, terms involving \bar{r}_k and $\tilde{a}_{k,d+1}$ are zero, since no action is taken at step k .

Algorithm 1 NM-PPG Training Procedure

- 1: **Input:** Fully observed dataset $\mathcal{D} = \{(x^{(i)}, y^{(i)})\}_{i=1}^n$, initial parameters (θ, ϕ) , trade-off parameter α , truncation horizon k , hard temperature τ_{hard} , soft-temperature schedule $(\tau_{\text{soft}}^{(1)}, \dots, \tau_{\text{soft}}^{(R)})$, entropy coefficient λ_{ent} , step sizes $(\eta_{\theta}, \eta_{\phi})$, maximum epochs per stage E , batch size B .
 - 2: Split \mathcal{D} into training and validation sets $\mathcal{D}_{\text{train}}$ and \mathcal{D}_{val} .
 - 3: Train predictor f_{ϕ} on $\mathcal{D}_{\text{train}}$ using random feature masks, see (2).
 - 4: $(\theta^*, \phi^*) \leftarrow (\theta, \phi)$.
 - 5: **for** $j = 1, \dots, R$ **do**
 - 6: Set $\tau_{\text{soft}} \leftarrow \tau_{\text{soft}}^{(j)}$.
 - 7: **for** $e = 1, \dots, E$ **do**
 - 8: **for each** minibatch $\mathcal{B} = \{(x^{(i)}, y^{(i)})\}_{i=1}^{|\mathcal{B}|} \subset \mathcal{D}_{\text{train}}$ of size B **do**
 - 9: **for** $i = 1, \dots, B$ **do** // Computed in parallel in practice.
 - 10: $(\bar{G}^{(i)}, \bar{H}^{(i)}, L_{\text{pred}}^{(i)}) \leftarrow \text{ST-ROLLOUT}(x^{(i)}, y^{(i)}, \theta, \phi, \alpha, k, \tau_{\text{hard}}, \tau_{\text{soft}})$. // Alg. 2
 - 11: **end for**
 - 12: $\bar{J}_{\text{ent}} \leftarrow \frac{1}{|\mathcal{B}|} \sum_{i=1}^{|\mathcal{B}|} (\bar{G}^{(i)} - \lambda_{\text{ent}} \bar{H}^{(i)})$, $L_{\text{pred}} \leftarrow \frac{1}{|\mathcal{B}|} \sum_{i=1}^{|\mathcal{B}|} L_{\text{pred}}^{(i)}$.
 - 13: $\theta \leftarrow \theta - \eta_{\theta} \nabla_{\theta} \bar{J}_{\text{ent}}$, $\phi \leftarrow \phi - \eta_{\phi} \nabla_{\phi} L_{\text{pred}}$.
 - 14: **end for**
 - 15: $L_{\text{val}}(\theta, \phi) \leftarrow \frac{1}{|\mathcal{D}_{\text{val}}|} \sum_{(x,y) \in \mathcal{D}_{\text{val}}} [\ell(f_{\phi}(x(m_{t_{\theta}}(x))), y) + \alpha c(m_{t_{\theta}}(x))]$.
 - 16: If $L_{\text{val}}(\theta, \phi) < L_{\text{val}}(\theta^*, \phi^*)$, **update** $(\theta^*, \phi^*) \leftarrow (\theta, \phi)$.
 - 17: Perform early-stopping check for stage j based on L_{val} (see main text).
 - 18: **end for**
 - 19: Set $(\theta, \phi) \leftarrow (\theta^*, \phi^*)$.
 - 20: **end for**
 - 21: **Return** (θ^*, ϕ^*) .
-

Appendix A.3 provides the proof of Proposition 1 and further discussion of each term in (11), while Appendix E gives additional details on the benefit of the ST procedure. The surrogate-gradient expression gives useful intuition about how gradient information flows through actions, masks, stop masses, and survival weights. In practice, however, we simply optimize \bar{J} by automatic differentiation, which targets the ST surrogate gradient $\nabla_{\theta}^{\text{ST}} \bar{J}$. This ST estimator is biased relative to the exact gradient of the hard-forward objective, but typically lower variance and more stable than score-function estimators [38, 42]. The resulting rollout trains policy and predictor on discrete masks, which better aligns optimization with deployment and reduces the relaxation gap, while still enabling pathwise gradients through the soft stopping and mask dynamics.

3.4 Training Procedure

Policy collapse, where the policy becomes prematurely overly deterministic and exploration deteriorates, is a common challenge in RL and is often addressed with entropy regularization, as in *maximum entropy* RL [41, 43]. We follow this approach and add an entropy bonus to the ST objective. Let $\mathcal{H}_t(\theta) \triangleq -\sum_{a \in \mathcal{A}} \pi_{\theta}(a | x(\bar{m}_t)) \log \pi_{\theta}(a | x(\bar{m}_t))$. For a single rollout, define $\bar{H}(x, y, \theta, \varepsilon) \triangleq \sum_{t=0}^{k-1} \tilde{s}_t \mathcal{H}_t(\theta)$. The final policy objective minimized by NM-PPG is

$$\bar{J}_{\text{ent}}(\theta) \triangleq \mathbb{E}_{\mathbf{x}, \mathbf{y}} \mathbb{E}_{\varepsilon} [\bar{G}(\mathbf{x}, \mathbf{y}, \theta, \varepsilon) - \lambda_{\text{ent}} \bar{H}(\mathbf{x}, \mathbf{y}, \theta, \varepsilon)], \quad (12)$$

where $\lambda_{\text{ent}} \geq 0$ controls the strength of entropy regularization. The entropy term encourages exploration during training, while the cost-loss trade-off itself is still determined by \bar{G} , which targets the standard AFA objective in (2).

Alg. 1 summarizes training for *non-myopic pathwise policy gradients* (NM-PPG), while Alg. 2 gives the single-instance ST rollout from Section 3.3. As described in Section 1, NM-PPG is model-free: it does not learn transition dynamics, but optimizes the acquisition policy directly from observed rollouts (see Appendix F.4). Training uses a fixed soft-temperature schedule. At each τ_{soft} , we train for at most E epochs and stop early when the deterministic validation loss L_{val} in line 15 has not improved for 100 epochs. We keep the globally best checkpoint (θ^*, ϕ^*) across all stages, restore it before moving to the next temperature, and return it as the final model. This avoids tuning both τ_{soft}

and the number of epochs for each dataset. We first train f_ϕ on random masks in accordance with (2). We then refine it on rollout-visited masks using L_{pred} , keeping the predictor aligned with the policy-induced state distribution. Further details on training and inference are given in Appendix B.

4 Experiments

In this section, we present our experimental setup and results. Additional details and extended results are in Appendix C.

Datasets. We evaluate on 12 datasets commonly used in previous work on AFA, spanning synthetic, real-world tabular, real-world medical, and real-world image settings. Synthetic datasets include two **Cube-NM** variants with $n_c = 5$ and $\sigma \in \{0.1, 0.2\}$ [31], and **Syn1** and **Syn3** (context-dependent synthetic benchmarks) [32]. Cube-NM, Syn1, and Syn3 are discussed in more detail below. Real-world tabular datasets are **Connect4** (game outcome prediction) [44], **Splice** (splice-junction classification) [45], and **Engine-FaultDB** (engine fault diagnosis) [46]. Real-world medical datasets are **Metabric** (breast cancer subtype prediction) [47, 48], **Mortality** (mortality prediction) [49], and **Diabetes** (diabetes diagnosis) [49]. Real-world image datasets are **MNIST** (digit image classification) [50] and **Fashion-MNIST** (clothing image classification) [51]. Non-uniform feature costs are used on Cube-NM, Mortality, and Diabetes; the remaining datasets use uniform unit feature costs. Table 2 in Appendix C.2 summarizes information about the datasets. Additional dataset details, including a motivation for their suitability in AFA where features are assumed costly, are provided in Appendix C.2.

Baselines. We compare our proposed method, **NM-PPG**, against the following baselines. Three myopic baselines: **DiFA** [23], **GDFS** [22], and **DIME** [24]. We explain myopic methods in the next subsection, and in more detail in Appendix C.1. Two methods from the non-myopic AFA literature that do not use explicit RL: **AACO** [12] and **SEFA** [32]. Two non-myopic RL methods: **GSMRL** [26] and **OL** [30]. GSMRL is model-based and uses PPO [52] as its RL optimizer, while OL is model-free and uses DQN [53]. See Appendix F.4 for how we use the term model-based in the AFA-POMDP. Full details for all baselines are provided in Appendix C.1.

Hyperparameters. For NM-PPG (Alg. 1), we use horizon $k = \min(d, 30)$ for all datasets. For fair comparison, we use the same horizon for all baselines where relevant; see Appendix C.1 for details. We set $\tau_{\text{hard}} = 1.0$ and train in stages with $\tau_{\text{soft}} \in \{0.8, 0.5, 0.2, 0.05, 0.02\}$ across all datasets. We set the maximum number of epochs per stage to $E = 2000$, but stop a stage early if the validation loss has not improved for 100 epochs. We set the policy learning rate to 10^{-3} , the predictor learning rate to 10^{-4} , and the entropy coefficient to $\lambda_{\text{ent}} = 0.5$. Both the predictor f_ϕ and policy π_θ (and other models for baselines) are implemented as neural networks. Remaining hyperparameters for all methods, including neural network architectures, are deferred to Appendix C.3.

Training and Evaluation. For each dataset, we split the data into training and test sets. For NM-PPG, training follows Alg. 1 and inference on test instances follows Alg. 3 (in Appendix B). See Appendix C.1 for training/evaluation details of baselines. Each experiment is repeated five times with different random seeds, and we report the mean with one-standard-deviation shading across runs. We report average acquisition cost and predictive performance on the test set. We use accuracy as the primary

Algorithm 2: ST Rollout for One Instance (x, y) .

- 1: **Input:** $x, y, \theta, \phi, \alpha, k, \tau_{\text{hard}}, \tau_{\text{soft}}$.
 - 2: Initialize $m_0 = \mathbf{0}, \tilde{m}_0 = \mathbf{0}, \tilde{m}_0 = \mathbf{0}$, and $\tilde{s}_0 = 1$.
 - 3: Initialize $\bar{G} \leftarrow 0, \bar{H} \leftarrow 0$, and $L_{\text{pred}} \leftarrow 0$.
 - 4: **for** $t = 0, \dots, k - 1$ **do**
 - 5: $z_t \leftarrow z_\theta(x(\tilde{m}_t))$.
 - 6: $z_{t,j} \leftarrow -\infty$ for all $j \in [d]$ with $m_{t,j} = 1$.
 - 7: $\pi_\theta(\cdot | x(\tilde{m}_t)) \leftarrow \text{softmax}(z_t/\tau_{\text{hard}})$.
 - 8: $\varepsilon_t \sim \text{Gumbel}(0, 1)^{d+1}$.
 - 9: $\tilde{a}_t \leftarrow \text{softmax}(((z_t/\tau_{\text{hard}}) + \varepsilon_t)/\tau_{\text{soft}})$.
 - 10: $\tilde{r}_t \leftarrow \text{softmax}(((z_{t,1:d}/\tau_{\text{hard}}) + \varepsilon_{t,1:d})/\tau_{\text{soft}})$.
 - 11: $r_t \leftarrow \text{onehot}(\text{argmax}_{j \in [d]}(\tilde{r}_{t,j}))$.
 - 12: $\bar{r}_t \leftarrow r_t - \text{sg}(\tilde{r}_t) + \tilde{r}_t, \ell_t \leftarrow \ell(f_\phi(x(\tilde{m}_t)), y)$.
 - 13: $\Delta_t \leftarrow \alpha(1 - \tilde{a}_{t,d+1}) \sum_{j=1}^d \bar{r}_{t,j} c(j) + \tilde{a}_{t,d+1} \ell_t$.
 - 14: $\bar{G} \leftarrow \bar{G} + \tilde{s}_t \Delta_t, L_{\text{pred}} \leftarrow L_{\text{pred}} + \ell_t$.
 - 15: $\bar{H} \leftarrow \bar{H} + \tilde{s}_t \mathcal{H}(\pi_\theta(\cdot | x(\tilde{m}_t)))$.
 - 16: $\tilde{m}_{t+1} \leftarrow \tilde{m}_t + (1 - \tilde{m}_t) \odot \tilde{r}_t$.
 - 17: $m_{t+1} \leftarrow m_t + (1 - m_t) \odot r_t$.
 - 18: $\tilde{m}_{t+1} \leftarrow m_{t+1} - \text{sg}(\tilde{m}_{t+1}) + \tilde{m}_{t+1}$.
 - 19: $\tilde{s}_{t+1} \leftarrow \tilde{s}_t(1 - \tilde{a}_{t,d+1})$.
 - 20: **end for**
 - 21: $\ell_k \leftarrow \ell(f_\phi(x(\tilde{m}_k)), y)$.
 - 22: $\bar{G} \leftarrow \bar{G} + \tilde{s}_k \ell_k, L_{\text{pred}} \leftarrow (L_{\text{pred}} + \ell_k)/(k + 1)$.
 - 23: **Return** $(\bar{G}, \bar{H}, L_{\text{pred}})$.
-

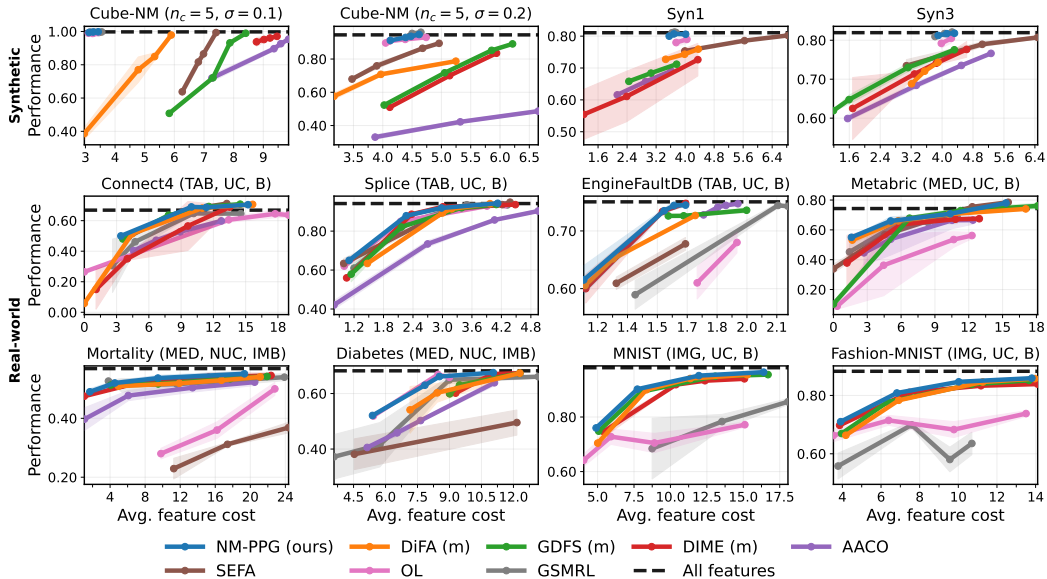


Figure 1: Results for all methods across synthetic (top row) and real-world (2 bottom rows) datasets. The row labels separate synthetic and real-world datasets. Performance is measured by accuracy for balanced datasets and F1-score for imbalanced datasets. The suffix (m) in the legend denotes myopic baselines. For real-world datasets, titles use the following acronyms: TAB/MED/IMG (tabular/medical/image), NUC/UC (non-uniform-cost/uniform-cost), and IMB/B (imbalanced/balanced).

metric on balanced datasets and F1-score on imbalanced datasets. Each point for each method in the performance plots corresponds to a different value of the trade-off parameter α , which yields a different trade-off between feature acquisition cost and predictive performance. Appendix C.3 explains how we choose α values, and Appendix C.1 clarifies how each baseline uses α .

4.1 Results and Discussion

Myopic vs. Non-Myopic AFA. A myopic AFA policy uses a local one-step lookahead: at each state, it compares stopping immediately with acquiring one additional feature and then stopping. This does not mean that the deployed policy is limited to one acquisition overall; the one-step rule can be applied repeatedly until the policy stops or reaches the maximum acquisition horizon. In contrast, a non-myopic policy optimizes over a longer future horizon, so an acquisition can be useful not because of its immediate predictive value, but because it changes which future acquisitions become informative and when the policy should stop. In our k -truncated objective, k is the maximum number of acquisitions. A non-myopic policy optimizes over the remaining $k - t$ steps at step t , whereas myopic methods use the same acquisition cap k but plan only one step ahead at each decision. Non-myopic planning is particularly important when features are jointly informative about the label but only weakly informative on their own (see concrete example below, and further discussion in Appendix G). Planning over a longer horizon naturally makes optimization more difficult, and NM-PPG can be trained with arbitrary horizons to balance this trade-off. Appendix C.1 explains how this distinction relates to the considered baselines.

Cube-NM was designed to expose this difference. In each instance, a hidden context determines which feature block contains label information. The context features identify the relevant block, but are themselves uninformative about the label. The parameter n_c denotes the number of possible contexts, and σ controls the noise level in the generated feature values; Appendix C.2 gives the full construction. Therefore, an optimal policy must first acquire the context features, whereas a myopic policy would not select them because they provide no immediate label information. This non-myopic structure is described in Appendix C.2, and Theorem 3 (adapted from [31]) shows that, on this dataset, non-myopic selection can require substantially fewer acquisitions than a myopic

policy. Syn1 and Syn3 have also been used in prior AFA work to evaluate non-myopic acquisition methods [32]. In both datasets, the feature x_{11} acts as a context variable: it is not directly predictive of the label, but it determines which later interaction block is informative. Thus, a non-myopic policy should acquire x_{11} early and then choose different follow-up features depending on its value, while a myopic policy is biased toward features with more immediate label information. These synthetic datasets highlight that *the advantage of using a longer planning horizon is dataset dependent*. When informative features contribute largely additively, or are immediately useful for predicting the label, a one-step lookahead policy may already be optimal. Thus, a useful non-myopic method should not only exploit long-horizon structure when it is present, but also recover the effectively myopic policy when that is optimal. As discussed below, NM-PPG does this more effectively than existing non-myopic baselines.

Non-Myopic Baselines. Existing non-myopic methods are known to be highly unstable, and are often outperformed by myopic baselines such as GDFS and DIME [22, 24, 31]. This applies broadly across non-myopic AFA methods, although for different reasons. RL-based methods directly optimize the sequential AFA-POMDP, but can suffer from high-variance policy-gradient learning. Non-RL non-myopic methods such as AACO and SEFA can be more stable because they do not optimize the full POMDP directly. Instead, they form acquisition policies by exploiting the AFA-specific observation that non-myopic selection requires reasoning about jointly informative features; see Appendix C.1 for details. However, this also makes them approximate and biased relative to long-term cost minimization in the AFA-POMDP, and they scale poorly to high-dimensional datasets. NM-PPG is designed to address these combined limitations: it uses the structure of AFA to obtain stable pathwise gradients while still targeting long-term cost minimization in the AFA-POMDP. As a result, it exploits non-myopic structure more effectively than existing methods, while remaining consistent with myopic baselines on many real-world datasets where myopic selection appears sufficient. No other method performs consistently well across all datasets.

Results on Synthetic Datasets. The first row of Figure 1 shows the results on the synthetic datasets. All features correspond to the performance of a predictor trained and evaluated with all features available on the respective dataset. NM-PPG is either consistent with or significantly better than existing non-myopic AFA methods and myopic baselines. All synthetic datasets contain explicit non-myopic structure, meaning that a non-myopic policy is required for optimal performance (see details about these datasets above). The strong performance on these datasets shows that NM-PPG can exploit non-myopic structure when it is present. Appendix C.5 confirms this by visualizing that NM-PPG recovers the intended context-first acquisition paths on Cube-NM, Syn1, and Syn3.

Results on Real-World Datasets. The second and third rows of Figure 1 show the results on the real-world datasets. AACO and SEFA are not included on image datasets, as they do not scale to high-dimensional datasets. NM-PPG is either consistent with or significantly better than existing non-myopic AFA methods. This is particularly clear on the high-dimensional image datasets MNIST and Fashion-MNIST, where NM-PPG remains stable while prior RL-based non-myopic methods are much less reliable, addressing a well-known limitation of earlier non-myopic AFA approaches. On some of the real-world datasets, NM-PPG has similar performance to the best performing myopic baselines. A likely explanation is that these datasets do not exhibit strong non-myopic structure, so a myopic acquisition policy is close to optimal; in such cases, NM-PPG recovers the stability of myopic selection rather than forcing unnecessary long-horizon behavior. On some medical datasets, however, we observe a clear benefit of NM-PPG over myopic baselines. Appendix C.5 shows that NM-PPG indeed learns different acquisition policies from the myopic methods on these datasets, requiring non-myopic reasoning, which explains the better performance.

Additional Experiments. Appendix C.4 reports ablation studies that investigate the benefit of the ST rollout procedure from Section 3.3 and the role of entropy regularization from Section 3.4. Appendix C.5 visualizes acquisition trajectories, showing that NM-PPG recovers the optimal non-myopic acquisition trajectories on synthetic datasets and finds non-myopic acquisition policies on two medical datasets that myopic policies do not recover. Appendix C.6 reports runtime results, Appendix C.7 analyzes training dynamics for NM-PPG, and Appendix C.8 separates the main results into comparisons against myopic and non-myopic baselines.

5 Conclusion

We introduced NM-PPG, a non-myopic AFA method for long-term cost minimization in the AFA-POMDP. Like RL-based non-myopic AFA methods, NM-PPG directly optimizes this long-term objective, but avoids generic RL estimators such as value-function learning or score-function policy gradients. Instead, it exploits the structure of AFA through a continuous relaxation of the acquisition process, which enables pathwise gradients through full acquisition trajectories (Section 3.2). We then reduce the gap between relaxed training and discrete deployment using an ST rollout (Section 3.3), and stabilize optimization with entropy regularization and staged temperature sharpening (Section 3.4). NM-PPG also avoids the main limitation of non-RL non-myopic AFA methods, which replace the sequential decision problem with an approximate proxy based on non-adaptive joint informativeness. The experiments in Section 4.1 show that NM-PPG (i) is more stable than existing non-myopic baselines, (ii) remains consistent with strong myopic baselines on datasets where myopic one-step acquisition is sufficient, and (iii) outperforms them when the dataset exhibits genuine non-myopic structure. Overall, NM-PPG provides a practical way to obtain non-myopic AFA policies while retaining much of the robustness that makes myopic methods attractive.

Acknowledgments

This work was partially supported by the Wallenberg AI, Autonomous Systems and Software Program (WASP) funded by the Knut and Alice Wallenberg Foundation. The computations and data handling was enabled by resources provided by the National Academic Infrastructure for Supercomputing in Sweden (NAISS), partially funded by the Swedish Research Council through grant agreement no. 2022-06725.

References

- [1] G. A. Gorry and G. O. Barnett. Experience with a model of sequential diagnosis. *Computers and Biomedical Research*, 1(5):490–507, 1968.
- [2] Arjan J. P. Jeckmans, Michael Beye, Zekeriya Erkin, Pieter Hartel, Reginald L. Legendijk, and Qiang Tang. *Privacy in Recommender Systems*. Springer London, 2013.
- [3] David Heckerman, John S. Breese, and Koos Rommelse. Decision-theoretic troubleshooting. *Commun. ACM*, 38(3):49–57, 1995.
- [4] Yuxin Chen, Jean-Michel Renders, Morteza Haghir Chehreghani, and Andreas Krause. Efficient online learning for optimizing value of information: Theory and application to interactive troubleshooting. In *Proceedings of the Thirty-Third Conference on Uncertainty in Artificial Intelligence*, 2017.
- [5] Cyrill Stachniss, Giorgio Grisetti, and Wolfram Burgard. Information gain-based exploration using rao-blackwellized particle filters. In *Proceedings of Robotics: Science and Systems (RSS)*, 2005.
- [6] Andreas Krause and Carlos Guestrin. Optimal value of information in graphical models. *J. Artif. Int. Res.*, 35:557–591, 2009.
- [7] Mikko Lauri, David Hsu, and Joni Pajarinen. Partially observable markov decision processes in robotics: A survey. *IEEE Transactions on Robotics*, 39(1):21–40, 2023.
- [8] Michael Cooper, Rohan Wadhawan, John Michael Giorgi, Chenhao Tan, and Davis Liang. The curious language model: Strategic test-time information acquisition. In *Second Workshop on Test-Time Adaptation: Putting Updates to the Test! at ICML 2025*, 2025.
- [9] Gabriel Dulac-Arnold, Ludovic Denoyer, Philippe Preux, and Patrick Gallinari. Datum-wise classification: A sequential approach to sparsity. In *Machine Learning and Knowledge Discovery in Databases*, 2011.
- [10] Linus Aronsson, Arman Rahbar, and Morteza Haghir Chehreghani. A survey on active feature acquisition strategies. *arXiv preprint arXiv:2502.11067*, 2026.

- [11] Isabelle Guyon and André Elisseeff. An introduction to variable and feature selection. *J. Mach. Learn. Res.*, 3:1157–1182, 2003. URL <https://jmlr.org/papers/v3/guyon03a.html>.
- [12] Michael Valancius, Maxwell Lennon, and Junier B. Oliva. Acquisition conditioned oracle for nongreedy active feature acquisition. In *Proceedings of the 41st International Conference on Machine Learning*, 2024.
- [13] K.J. Åström. Optimal control of markov processes with incomplete state information. *Journal of Mathematical Analysis and Applications*, 10(1):174–205, 1965.
- [14] Stéphane Ross, Joelle Pineau, Sébastien Paquet, and Brahim Chaib-draa. Online planning algorithms for pomdps. *J. Artif. Int. Res.*, 32:663–704, 2008.
- [15] David Silver and Joel Veness. Monte-carlo planning in large pomdps. In *Advances in Neural Information Processing Systems*, 2010.
- [16] Donald Geman and Bruno Jedynak. An active testing model for tracking roads in satellite images. *IEEE Transactions on Pattern Analysis and Machine Intelligence*, 18(1):1–14, 1996.
- [17] Xiaoyong Chai, Lin Deng, Qiang Yang, and Charles X Ling. Test-cost sensitive naive bayes classification. In *Fourth IEEE International Conference on Data Mining (ICDM'04)*, 2004.
- [18] Mustafa Bilgic and Lise Getoor. Voila: efficient feature-value acquisition for classification. In *Proceedings of the 22nd National Conference on Artificial Intelligence*, 2007.
- [19] Chao Ma, Sebastian Tschiatschek, Konstantina Palla, Jose Miguel Hernandez-Lobato, Sebastian Nowozin, and Cheng Zhang. Eddi: Efficient dynamic discovery of high-value information with partial VAE. In *International Conference on Machine Learning*. PMLR, 2019.
- [20] He He, Jason Eisner, and Hal Daume. Imitation learning by coaching. In *Advances in Neural Information Processing Systems*, 2012.
- [21] Jaromír Janisch, Tomáš Pevný, and Viliam Lisý. Classification with costly features as a sequential decision-making problem. *Mach. Learn.*, 109(8):1587–1615, 2020.
- [22] Ian Covert, Wei Qiu, Mingyu Lu, Nayoon Kim, Nathan White, and Su-In Lee. Learning to maximize mutual information for dynamic feature selection. In *Proceedings of the 40th International Conference on Machine Learning*, 2023.
- [23] Aritra Ghosh and Andrew Lan. Difa: Differentiable feature acquisition. *Proceedings of the AAAI Conference on Artificial Intelligence*, 2023.
- [24] Soham Gadgil, Ian Connick Covert, and Su-In Lee. Estimating conditional mutual information for dynamic feature selection. In *The Twelfth International Conference on Learning Representations*, 2024. URL <https://openreview.net/forum?id=0ju2Qu9jvn>.
- [25] Sara Zannone, Jose Miguel Hernandez Lobato, Cheng Zhang, and Konstantina Palla. Odin: Optimal discovery of high-value information using model-based deep reinforcement learning. In *Real-world Sequential Decision Making Workshop, ICML*, 2019.
- [26] Yang Li and Junier Oliva. Active feature acquisition with generative surrogate models. In *Proceedings of the 38th International Conference on Machine Learning*, 2021.
- [27] Yang Li and Junier Oliva. Distribution guided active feature acquisition. *arXiv preprint arXiv:2410.03915*, 2024.
- [28] Osman Berke Guney, Ketan Suhaas Saichandran, Karim Elzokm, Ziming Zhang, and Vijaya B Kolachalama. Active feature acquisition via explainability-driven ranking. In *Forty-second International Conference on Machine Learning*, 2025.
- [29] Hajin Shim, Sung Ju Hwang, and Eunho Yang. Joint active feature acquisition and classification with variable-size set encoding. In *Advances in Neural Information Processing Systems*, 2018.

- [30] Mohammad Kachuee, Orpaz Goldstein, Kimmo Kärkkäinen, and Majid Sarrafzadeh. Opportunistic learning: Budgeted cost-sensitive learning from data streams. In *International Conference on Learning Representations*, 2019.
- [31] Valter Schütz, Han Wu, Reza Rezvan, Linus Aronsson, and Morteza Haghiri Chehreghani. Afabench: A generic framework for benchmarking active feature acquisition. *arXiv preprint arXiv:2508.14734*, 2026.
- [32] Alexander Luke Ian Norcliffe, Changhee Lee, Fergus Imrie, Mihaela van der Schaar, and Pietro Lio. Stochastic encodings for active feature acquisition. In *Forty-second International Conference on Machine Learning*, 2025.
- [33] Aditya Chattopadhyay, Kwan Ho Ryan Chan, Benjamin David Haeffele, Donald Geman, and Rene Vidal. Variational information pursuit for interpretable predictions. In *The Eleventh International Conference on Learning Representations*, 2023. URL <https://openreview.net/forum?id=771SWa-Tm3Z>.
- [34] T. Rückstieß, C. Osendorfer, and P. van der Smagt. Minimizing data consumption with sequential online feature selection. *International Journal of Machine Learning and Cybernetics*, 4:235–243, 2013.
- [35] Richard S. Sutton and Andrew G. Barto. *Reinforcement Learning: An Introduction*. Adaptive Computation and Machine Learning series. The MIT Press, 2 edition, 2018.
- [36] Shakir Mohamed, Mihaela Rosca, Michael Figurnov, and Andriy Mnih. Monte carlo gradient estimation in machine learning. *Journal of Machine Learning Research*, 2020.
- [37] Claas A Voelcker, Axel Brunnbauer, Marcel Hussing, Michal Nauman, Pieter Abbeel, Radu Grosu, Eric Eaton, Amir massoud Farahmand, and Igor Gilitschenski. Relative entropy pathwise policy optimization. In *The Fourteenth International Conference on Learning Representations*, 2026.
- [38] Eric Jang, Shixiang Gu, and Ben Poole. Categorical reparameterization with gumbel-softmax. In *International Conference on Learning Representations*, 2017.
- [39] Chris J. Maddison, Andriy Mnih, and Yee Whye Teh. The concrete distribution: A continuous relaxation of discrete random variables. In *International Conference on Learning Representations*, 2017.
- [40] David Silver, Guy Lever, Nicolas Heess, Thomas Degris, Daan Wierstra, and Martin Riedmiller. Deterministic policy gradient algorithms. In *Proceedings of the 31st International Conference on Machine Learning*, 2014.
- [41] Tuomas Haarnoja, Aurick Zhou, Pieter Abbeel, and Sergey Levine. Soft actor-critic: Off-policy maximum entropy deep reinforcement learning with a stochastic actor. In *Proceedings of the 35th International Conference on Machine Learning*, 2018.
- [42] Yoshua Bengio, Nicholas Léonard, and Aaron Courville. Estimating or propagating gradients through stochastic neurons for conditional computation. *arXiv preprint arXiv:1308.3432*, 2013.
- [43] Brian D. Ziebart, Andrew Maas, J. Andrew Bagnell, and Anind Dey. Maximum entropy inverse reinforcement learning. In *Proceedings of the 23rd AAAI Conference on Artificial Intelligence*, pages 1433–1438, 2008.
- [44] John Tromp. Connect-4. UCI Machine Learning Repository, 1995. DOI: <https://doi.org/10.24432/C59P43>.
- [45] Molecular Biology (Splice-junction Gene Sequences). UCI Machine Learning Repository, 1991. DOI: <https://doi.org/10.24432/C5M888>.
- [46] Mary Vergara, Leo Ramos, Néstor Diego Rivera-Campoverde, and Francklin Rivas-Echeverría. Enginefaultdb: A novel dataset for automotive engine fault classification and baseline results. *IEEE Access*, 11:126155–126171, 2023. doi: 10.1109/ACCESS.2023.3331316.

- [47] Christina Curtis, Sohrab P. Shah, Suet-Feung Chin, et al. The genomic and transcriptomic architecture of 2,000 breast tumours reveals novel subgroups. *Nature*, 486(7403):346–352, 2012. doi: 10.1038/nature10983.
- [48] Bernard Pereira, Suet-Feung Chin, Oscar M. Rueda, et al. The somatic mutation profiles of 2,433 breast cancers refine their genomic and transcriptomic landscapes. *Nature Communications*, 7: 11479, 2016. doi: 10.1038/ncomms11479.
- [49] Centers for Disease Control and Prevention. National health and nutrition examination survey (nhanes). <https://www.cdc.gov/nchs/nhanes/>, 2026. Accessed: 2026-04-08.
- [50] Yann LeCun, Léon Bottou, Yoshua Bengio, and Patrick Haffner. Gradient-based learning applied to document recognition. *Proceedings of the IEEE*, 86(11):2278–2324, 1998.
- [51] Han Xiao, Kashif Rasul, and Roland Vollgraf. Fashion-mnist: a novel image dataset for benchmarking machine learning algorithms. *arXiv preprint arXiv:1708.07747*, 2017.
- [52] John Schulman, Filip Wolski, Prafulla Dhariwal, Alec Radford, and Oleg Klimov. Proximal policy optimization algorithms. *arXiv preprint arXiv:1707.06347*, 2017.
- [53] Volodymyr Mnih, Koray Kavukcuoglu, David Silver, Andrei A Rusu, Joel Veness, Marc G Bellemare, Alex Graves, Martin Riedmiller, Andreas K Fidjeland, Georg Ostrovski, et al. Human-level control through deep reinforcement learning. *nature*, 518(7540):529–533, 2015.
- [54] Gabriel Erion, Joseph D. Janizek, Carly Hudelson, Richard B. Utarnachitt, Andrew M. McCoy, Michael R. Sayre, Nathan J. White, and Su-In Lee. A cost-aware framework for the development of ai models for healthcare applications. *Nature Biomedical Engineering*, 6:1384–1398, 2022. doi: 10.1038/s41551-022-00872-8.
- [55] Paul Viola and Michael J. Jones. Robust real-time face detection. *International Journal of Computer Vision*, 57(2):137–154, 2004.
- [56] Diederik P. Kingma and Jimmy Ba. Adam: A method for stochastic optimization. In *International Conference on Learning Representations (ICLR)*, 2015.
- [57] Marine Le Morvan, Julie Josse, Thomas Moreau, Erwan Scornet, and Gael Varoquaux. Neumiss networks: differentiable programming for supervised learning with missing values. In *Advances in Neural Information Processing Systems*, volume 33, 2020.

A Proofs

A.1 Proof of Theorem 1

By construction of the AFA-POMDP in Section 3.1, the one-step cost is

$$C((m_t, x, y), a) = \begin{cases} \alpha c(a), & a \in [d], \\ \ell(f_\phi(x(m_t)), y), & a = d + 1. \end{cases} \quad (13)$$

Let $t_\theta(x)$ be the policy-induced first stopping step, so $a_{t_\theta(x)} = d + 1$. The trajectory return is

$$G(x, y, \pi_\theta) = \sum_{t=0}^{t_\theta(x)-1} \alpha c(a_t) + \ell(f_\phi(x(m_{t_\theta(x)})), y). \quad (14)$$

Because $m_{t_\theta(x)}$ records exactly the features acquired before stopping, $c(m_{t_\theta(x)}) = \sum_{t=0}^{t_\theta(x)-1} c(a_t)$. Hence

$$G(x, y, \pi_\theta) = \alpha c(m_{t_\theta(x)}) + \ell(f_\phi(x(m_{t_\theta(x)})), y). \quad (15)$$

Taking expectations over (\mathbf{x}, \mathbf{y}) and policy rollouts gives

$$J(\pi_\theta) = \mathbb{E}_{\mathbf{x}, \mathbf{y}} \mathbb{E}_{\pi_\theta} [\ell(f_\phi(\mathbf{x}(m_{t_\theta(\mathbf{x})))), \mathbf{y}) + \alpha c(m_{t_\theta(\mathbf{x})})], \quad (16)$$

which is exactly the standard AFA objective in (2). \square

A.2 Proof of Theorem 2

We now prove property (i). We show that $\tilde{m}_t \in [0, 1]^d$ for all t . We prove this coordinate-wise by induction. At $t = 0$, we initialize $\tilde{m}_0 = \mathbf{0}$, so every coordinate lies in $[0, 1]$. Now assume $\tilde{m}_{t,j} \in [0, 1]$ for some step t and coordinate j . Since \tilde{r}_t is a softmax over feature logits, $\tilde{r}_{t,j} \in [0, 1]$. The mask update in (7) gives

$$\tilde{m}_{t+1,j} = \tilde{m}_{t,j} + (1 - \tilde{m}_{t,j})\tilde{r}_{t,j}. \quad (17)$$

Because $1 - \tilde{m}_{t,j} \geq 0$ and $\tilde{r}_{t,j} \geq 0$, it follows that $\tilde{m}_{t+1,j} \geq \tilde{m}_{t,j} \geq 0$. For the upper bound,

$$\tilde{m}_{t+1,j} = \tilde{m}_{t,j} + (1 - \tilde{m}_{t,j})\tilde{r}_{t,j} \leq \tilde{m}_{t,j} + (1 - \tilde{m}_{t,j}) \cdot 1 = 1. \quad (18)$$

Hence $\tilde{m}_{t+1,j} \in [0, 1]$. By induction, every coordinate of \tilde{m}_t remains in $[0, 1]$ for all t , and therefore $\tilde{m}_t \in [0, 1]^d$ for all t .

We now prove property (ii). From the recursion $\tilde{s}_{t+1} = \tilde{s}_t(1 - \tilde{a}_{t,d+1})$, we have

$$\tilde{s}_t \tilde{a}_{t,d+1} = \tilde{s}_t - \tilde{s}_t(1 - \tilde{a}_{t,d+1}) = \tilde{s}_t - \tilde{s}_{t+1}. \quad (19)$$

Therefore, the stop-time masses satisfy

$$\sum_{t=0}^{k-1} \tilde{s}_t \tilde{a}_{t,d+1} + \tilde{s}_k = \sum_{t=0}^{k-1} (\tilde{s}_t - \tilde{s}_{t+1}) + \tilde{s}_k = ((\tilde{s}_0 - \tilde{s}_1) + (\tilde{s}_1 - \tilde{s}_2) + \dots + (\tilde{s}_{k-1} - \tilde{s}_k)) + \tilde{s}_k = \tilde{s}_0 = 1, \quad (20)$$

where the intermediate terms cancel telescopically, and the last equality uses the initialization $\tilde{s}_0 = 1$ from (7). Thus the induced stop-time masses form a valid distribution over the stopping step.

We now prove property (iii). Assume $\tilde{a}_t \in \{e_1, \dots, e_{d+1}\}$ for each t . Let $t_\theta(x)$ be the first step $t < k$ such that $\tilde{a}_{t,d+1} = 1$, with $t_\theta(x) = k$ if no such step occurs. For every continuation step $t < t_\theta(x)$, the hard action must be a feature acquisition. We denote this feature by $a_t \in [d]$. Then $\tilde{a}_{t,d+1} = 0$, $1 - \tilde{a}_{t,d+1} = 1$, and the conditional feature-acquisition distribution satisfies $\tilde{r}_t = e_{a_t}$. Because acquired feature logits are blocked, no feature action can be selected more than once. Hence the mask update in (7) reduces to

$$\tilde{m}_{t+1} = \tilde{m}_t + (1 - \tilde{m}_t) \odot e_{a_t}, \quad (21)$$

which is exactly the discrete feature-acquisition update. Therefore, by induction, $\tilde{m}_t = m_t$ for all $t \leq t_\theta(x)$. If $t_\theta(x) \leq k - 1$, then at the stopping step $\tilde{a}_{t_\theta(x),d+1} = 1$, so $\tilde{s}_{t_\theta(x)+1} = 0$. The feature distribution at the stopping step is immaterial: the acquisition-cost multiplier $1 - \tilde{a}_{t_\theta(x),d+1}$ is zero. If the recursion is formally unrolled after this hard stop, all later terms in (8) have zero survival mass and therefore do not affect \tilde{G} . If no earlier stop occurs, then $t_\theta(x) = k$, and the same argument gives $\tilde{m}_t = m_t$ for all $t \leq k$. The survival variables satisfy

$$\tilde{s}_t = \begin{cases} 1, & t \leq t_\theta(x), \\ 0, & t > t_\theta(x), \end{cases} \quad (22)$$

In the hard case, this stop-time distribution is degenerate: exactly one stop mass is equal to 1. If stopping occurs at some $t_\theta(x) \leq k - 1$, then $\tilde{s}_{t_\theta(x)} = 1$, $\tilde{a}_{t_\theta(x),d+1} = 1$, and all remaining masses are zero. If no earlier stop occurs, then $\tilde{s}_k = 1$.

Therefore, the acquisition-cost part in (8) becomes

$$\sum_{t=0}^{k-1} \tilde{s}_t \alpha (1 - \tilde{a}_{t,d+1}) c(\tilde{r}_t) = \sum_{t=0}^{t_\theta(x)-1} \alpha c(a_t), \quad (23)$$

since before stopping $\tilde{a}_{t,d+1} = 0$ and $\tilde{r}_t = e_{a_t}$, at the stopping step $1 - \tilde{a}_{t,d+1} = 0$, and after stopping $\tilde{s}_t = 0$. When $\tilde{a}_{t,d+1} = 1$, the conditional feature distribution \tilde{r}_t is immaterial because the continuation branch has zero mass. For the terminal-loss part,

$$\sum_{t=0}^{k-1} \tilde{s}_t \tilde{a}_{t,d+1} \tilde{\ell}_t + \tilde{s}_k \tilde{\ell}_k = \tilde{\ell}_{t_\theta(x)}, \quad (24)$$

because exactly one stop mass is active: either at some $t_\theta(x) \leq k - 1$ via $\tilde{s}_{t_\theta(x)} \tilde{a}_{t_\theta(x), d+1} = 1$, or at k via $\tilde{s}_k = 1$ if no earlier stop occurs. Since $\tilde{m}_{t_\theta(x)} = m_{t_\theta(x)}$, we also have $\tilde{\ell}_{t_\theta(x)} = \ell(f_\phi(x(m_{t_\theta(x)})), y)$. Hence

$$\tilde{G}(x, y, \theta, \varepsilon) = \ell(f_\phi(x(m_{t_\theta(x)})), y) + \sum_{t=0}^{t_\theta(x)-1} \alpha c(a_t) = G(x, y, \pi_\theta), \quad (25)$$

Taking expectation over (x, y) and policy randomness gives $\tilde{J}(\theta) = J(\pi_\theta)$.

We now prove property (iv). Fix (x, y) and a realization of the Gumbel noise. We prove convergence by induction over rollout steps. The base case is immediate because \tilde{m}_0 is fixed. Assume that $\tilde{m}_t(\tau_{\text{soft}})$ converges as $\tau_{\text{soft}} \rightarrow 0$. Since the masked input map and policy network are continuous in \tilde{m}_t , the logits $z_t(\tau_{\text{soft}}) = z_\theta(x(\tilde{m}_t(\tau_{\text{soft}})))$ also converge. Define $v_t(\tau_{\text{soft}}) \triangleq z_t(\tau_{\text{soft}})/\tau_{\text{hard}} + \varepsilon_t$, and let v_t^0 be its limit. Because the Gumbel distribution has a continuous density, v_t^0 has a unique maximizer almost surely. Let $i_t^* = \arg \max_i v_{t,i}^0$. Then the softmax defining \tilde{a}_t concentrates on this unique maximizer:

$$\tilde{a}_t(\tau_{\text{soft}}) \rightarrow e_{i_t^*} \quad \text{almost surely as } \tau_{\text{soft}} \rightarrow 0. \quad (26)$$

The same argument applied to the feature-only logits $z_{t,1:d}(\tau_{\text{soft}})/\tau_{\text{hard}} + \varepsilon_{t,1:d}$ shows that \tilde{r}_t converges almost surely to a one-hot feature action. The recursions in (7) are continuous in \tilde{m}_t, \tilde{r}_t , and $\tilde{a}_{t,d+1}$, so \tilde{m}_{t+1} and \tilde{s}_{t+1} also converge. This completes the induction. Therefore the relaxed actions become hard almost surely as $\tau_{\text{soft}} \rightarrow 0$. \square

A.3 Proof of Proposition 1 and Further Gradient Details

Proof. We derive the fixed-rollout ST surrogate gradient in Proposition 1 by applying the multivariate chain rule to the no-stop straight-through rollout computation graph used by NM-PPG. This is the derivative computed through the stop-gradient graph, not the exact derivative of the hard-forward objective. We use the same compact notation as in Section 3.3; vector-Jacobian contractions are left implicit.

Fix one realization (x, y, ε) , and define

$$g_{\text{ST}}(\theta) \triangleq \tilde{G}(x, y, \theta, \varepsilon). \quad (27)$$

Unlike the discrete deployment policy, the training rollout does not sample a hard stop action. Instead, at every step $t < k$, it samples a hard feature action r_t from the feature logits conditioned on not stopping. The relaxed stop masses $\tilde{a}_{t,d+1}$ and survival weights \tilde{s}_t then determine how much each stopping time contributes to the objective. Thus, for the ST pathwise derivative, $g_{\text{ST}}(\theta)$ is treated as a function of the variables

$$(\bar{r}_t, \bar{m}_t, \tilde{a}_{t,d+1}, \tilde{s}_t)_{t=0}^k, \quad (28)$$

where the terms involving \bar{r}_k and $\tilde{a}_{k,d+1}$ are dummy terminal terms whose derivatives are zero. The dependence on θ enters through the policy logits $z_t = z_\theta(x(\bar{m}_t))$, the Gumbel-Softmax samples \tilde{a}_t , the conditional feature distributions \tilde{r}_t , and the relaxed mask and survival recursions.

Equivalently, there is a scalar function F such that

$$g_{\text{ST}}(\theta) = F((\bar{r}_t(\theta), \bar{m}_t(\theta), \tilde{a}_{t,d+1}(\theta), \tilde{s}_t(\theta))_{t=0}^k). \quad (29)$$

This representation is useful because F has no additional explicit dependence on θ once (x, y, ε) is fixed: all dependence on θ is mediated by the rollout variables. Importantly, this does not assume that the variables u_0, \dots, u_k are independent. They may be coupled through the rollout recursion; the chain rule only treats them as formal arguments of F , while their coupling is captured by the total derivatives $\partial u_t / \partial \theta$. Thus, for any scalar composition $h(\theta) = F(u_0(\theta), \dots, u_k(\theta))$, the multivariate chain rule gives $\nabla_\theta h(\theta) = \sum_{t=0}^k (\partial F / \partial u_t) (\partial u_t / \partial \theta)$. Taking $u_t = (\bar{r}_t, \bar{m}_t, \tilde{a}_{t,d+1}, \tilde{s}_t)$ and expanding this vector into its components gives

$$\nabla_\theta^{\text{ST}} g_{\text{ST}}(\theta) = \sum_{t=0}^k \left(\frac{\partial \tilde{G}}{\partial \bar{r}_t} \frac{\partial \bar{r}_t}{\partial \theta} + \frac{\partial \tilde{G}}{\partial \bar{m}_t} \frac{\partial \bar{m}_t}{\partial \theta} + \frac{\partial \tilde{G}}{\partial \tilde{a}_{t,d+1}} \frac{\partial \tilde{a}_{t,d+1}}{\partial \theta} + \frac{\partial \tilde{G}}{\partial \tilde{s}_t} \frac{\partial \tilde{s}_t}{\partial \theta} \right). \quad (30)$$

Here, each partial derivative of \tilde{G} is taken with respect to one explicit argument of the scalar rollout objective in (10), while holding the other arguments fixed. Dependencies across time are therefore

not omitted: for example, the fact that \bar{m}_{t+1} depends on earlier acquisitions affects $\partial\bar{m}_{t+1}/\partial\theta$, not the partial derivative $\partial\bar{G}/\partial\bar{m}_{t+1}$. The same applies to \bar{r}_t , $\tilde{a}_{t,d+1}$, and \tilde{s}_t , since these variables are all produced by the recursively unrolled rollout. The terminal mask and survival contributions are included through the $t = k$ terms; the terminal action terms are zero because no feature is acquired and no stop probability is sampled at step k .

The straight-through definitions are

$$\bar{r}_t = r_t - \text{sg}(\tilde{r}_t) + \tilde{r}_t, \quad \bar{m}_t = m_t - \text{sg}(\tilde{m}_t) + \tilde{m}_t. \quad (31)$$

Since $\text{sg}(\cdot)$ has zero derivative, the backward pass satisfies

$$\frac{\partial\bar{r}_t}{\partial\tilde{r}_t} = I, \quad \frac{\partial\bar{m}_t}{\partial\tilde{m}_t} = I, \quad (32)$$

and therefore

$$\frac{\partial\bar{r}_t}{\partial\theta} = \frac{\partial\bar{r}_t}{\partial\tilde{r}_t} \frac{\partial\tilde{r}_t}{\partial\theta}, \quad \frac{\partial\bar{m}_t}{\partial\theta} = \frac{\partial\bar{m}_t}{\partial\tilde{m}_t} \frac{\partial\tilde{m}_t}{\partial\theta}. \quad (33)$$

Substituting these ST identities into the total derivative gives

$$\nabla_{\theta}^{\text{ST}} g_{\text{ST}}(\theta) = \sum_{t=0}^k \left(\frac{\partial\bar{G}}{\partial\bar{r}_t} \frac{\partial\bar{r}_t}{\partial\tilde{r}_t} \frac{\partial\tilde{r}_t}{\partial\theta} + \frac{\partial\bar{G}}{\partial\tilde{a}_{t,d+1}} \frac{\partial\tilde{a}_{t,d+1}}{\partial\theta} + \frac{\partial\bar{G}}{\partial\bar{m}_t} \frac{\partial\bar{m}_t}{\partial\tilde{m}_t} \frac{\partial\tilde{m}_t}{\partial\theta} + \frac{\partial\bar{G}}{\partial\tilde{s}_t} \frac{\partial\tilde{s}_t}{\partial\theta} \right). \quad (34)$$

This is exactly the ST surrogate-gradient expression in Proposition 1. The forward sampling rule for r_t is described in Section 3.2 and Appendix D; it is not differentiated through in the ST gradient.

The remaining derivatives are determined by the relaxed dynamics:

$$\tilde{m}_{t+1} = \tilde{m}_t + (1 - \tilde{m}_t) \odot \tilde{r}_t, \quad \tilde{s}_{t+1} = \tilde{s}_t(1 - \tilde{a}_{t,d+1}), \quad (35)$$

with $\tilde{m}_0 = 0$, $\tilde{s}_0 = 1$, and \tilde{a}_t given by the reparameterized sample in (4). Hence

$$\frac{\partial\tilde{m}_{t+1}}{\partial\theta} = (I - \text{Diag}(\tilde{r}_t)) \frac{\partial\tilde{m}_t}{\partial\theta} + \text{Diag}(1 - \tilde{m}_t) \frac{\partial\tilde{r}_t}{\partial\theta}, \quad (36)$$

$$\frac{\partial\tilde{s}_{t+1}}{\partial\theta} = (1 - \tilde{a}_{t,d+1}) \frac{\partial\tilde{s}_t}{\partial\theta} - \tilde{s}_t \frac{\partial\tilde{a}_{t,d+1}}{\partial\theta}. \quad (37)$$

These recursions show how an acquisition decision at an early step affects all later masks, stop masses, survival weights, costs, and terminal-loss terms. In practice, the expression above is evaluated by automatic differentiation through Alg. 2. \square

B Training and Inference Procedure

The overall NM-PPG training procedure and single-instance ST rollout are given in Alg. 1 and Alg. 2 in Section 3.4. As described in Section 1, NM-PPG belongs to the model-free category of AFA methods: it does not learn a model of the transition dynamics, but instead optimizes the acquisition policy directly from observed rollouts (see Appendix F.4). We train NM-PPG in stages over a fixed soft-temperature schedule. For each value of τ_{soft} , we train for at most E epochs, but stop the stage early if the validation loss L_{val} computed in line 15 has not improved for 100 epochs. The validation loss is computed using the deterministic policy rollout, analogous to the inference procedure in Alg. 3, which is also used for test evaluation. Throughout all stages, we maintain a single global best checkpoint (θ^*, ϕ^*) , defined as the policy and predictor with the smallest validation loss observed so far. After each stage, we restore this checkpoint before continuing with the next temperature, and the same checkpoint is returned as the final model. This avoids having to tune both τ_{soft} and the number of epochs separately for each dataset. The procedure begins by training the predictor f_{ϕ} on randomly sampled masks, in accordance with the optimization problem in (2). For each minibatch, we perform ST rollouts for all instances in parallel and update (θ, ϕ) accordingly. For each instance i , the rollout in line 10 returns the ST trajectory objective $\bar{G}^{(i)}$, the entropy term $\bar{H}^{(i)}$, and the predictor loss $L_{\text{pred}}^{(i)} = \frac{1}{k+1} \sum_{t=0}^k \ell(f_{\phi}(x^{(i)}(\bar{m}_t)), y^{(i)})$. This second stage of predictor training refines f_{ϕ} on masks encountered during policy rollouts, keeping it aligned with the policy-induced state distribution rather than only with uniformly sampled masks.

Alg. 3 gives the corresponding inference procedure for a single test instance. It applies the trained policy greedily, blocks already acquired features, and outputs the predictor label once the stop action is selected or the horizon is reached.

Algorithm 3 NM-PPG Inference for One Test Instance x .

```
1: Input: test instance  $x$ , trained predictor  $f_\phi$ , trained policy parameters  $\theta$ , horizon  $k$ .
2: Output: prediction  $\hat{y}$ .
3: Initialize  $m_0 = \mathbf{0}$ .
4: for  $t = 0, \dots, k - 1$  do
5:    $z_t \leftarrow z_\theta(x(m_t))$ .
6:    $z_{t,j} \leftarrow -\infty$  for all feature indices  $j \in [d]$  with  $m_{t,j} = 1$ .
7:    $a_t \leftarrow \arg \max_{i \in [d+1]} \text{softmax}(z_t)_i$ .
8:   if  $a_t = d + 1$  then
9:      $\hat{y} \leftarrow \arg \max f_\phi(x(m_t))$ .
10:    return  $\hat{y}$ .
11:  end if
12:   $m_{t+1} \leftarrow m_t + (1 - m_t) \odot \text{onehot}(a_t)$ .
13: end for
14: // Forced terminal prediction at horizon  $k$ .
15:  $\hat{y} \leftarrow \arg \max f_\phi(x(m_k))$ .
16: return  $\hat{y}$ .
```

C Experiments: More Details and Further Results

Experiments were conducted on shared compute clusters with NVIDIA A40 GPUs (48GB memory), although the full 48GB memory was not required for the runs reported here. GPU-based runs used one A40 GPU and corresponded to a single choice of method, dataset, trade-off parameter, and random seed. AACO was run on CPU workers because it is non-parametric and does not use GPU acceleration. Many runs were executed in parallel on the clusters.

C.1 Description of Baseline Methods

For all baselines, we use the publicly available implementations released by the original authors.

There are two common experimental settings in AFA. In the *hard-budget* setting, a fixed per-instance acquisition budget $\kappa > 0$ is chosen in advance, and each method acquires features for each instance until this budget is reached. The predictor is then evaluated at the resulting mask. This corresponds to minimizing prediction loss subject to a per-instance acquisition-cost constraint:

$$\min_{\theta} \mathbb{E}_{\mathbf{x}, \mathbf{y}} \mathbb{E}_{\pi_{\theta}} [\ell(f_{\phi}(\mathbf{x}(m_{t_{\theta}}(\mathbf{x}))), \mathbf{y})] \quad \text{s.t.} \quad c(m_{t_{\theta}}(x)) \leq \kappa \text{ for each instance } x. \quad (38)$$

In the uniform-cost case, this corresponds to acquiring a fixed number of features for every instance. In the *soft-budget* setting used in this paper, the method may stop at different times for different instances and is evaluated by the cost-loss objective in (2). Thus, the number of acquired features is part of the policy decision, and α controls the cost penalty in the same objective as prediction loss. This lets us compare full cost-performance curves rather than predictive performance at a fixed acquisition count.

Following prior AFA comparisons, and in particular the recommendation of the recent AFA benchmark [31], we adapt all methods to the soft-budget setting in (2), which is the setting we focus on in this paper, rather than evaluating some methods with a fixed hard budget and others with (2). Mixing these settings would conflate differences between algorithms with differences between evaluation objectives. For baselines that were originally proposed for the hard-budget setting, we also checked the performance of these methods using their original hard-budget formulation, but found that the adaptation to (2) performed better on the validation split. A likely reason is that the adapted variant does not force the method to exhaust the full budget for every instance, but can stop early when the predictor is sufficiently confident about the label; we therefore use the adapted version in all experiments. Below, we explain how each baseline method is adapted to (2), when adaptation is needed, and hence how α is used for each method.

C.1.1 Myopic Baselines

The AFA-POMDP used in this paper is formally defined in Appendix F. The immediate costs are chosen so that the induced expected return matches the standard AFA objective in (2). In particular, (71) gives the corresponding 1-step truncated value function used to describe myopic baselines.

Myopic methods are common in AFA because the full non-myopic problem is generally intractable: exact planning must reason over all future feature subsets and all possible future observations. They avoid this by asking only whether the policy should stop now or acquire one additional feature and then stop. The one-step state-action value is defined over all feasible actions $\mathcal{A}(S_t) = U_t \cup \{d+1\}$, including the stop action. For a candidate acquisition $a \in U_t$, let $m_{t+1} = m_t + (1 - m_t) \odot \text{onehot}(a)$. Then, for (2), this gives

$$\begin{aligned} Q_1(x(m_t), d+1) &= \mathbb{E}_{\mathbf{y}|x_{S_t}} [\ell(f_\phi(x(m_t)), \mathbf{y})], \\ Q_1(x(m_t), a) &= \alpha c(a) + \mathbb{E}_{\mathbf{x}_a, \mathbf{y}|x_{S_t}} [\ell(f_\phi(\mathbf{x}(m_{t+1})), \mathbf{y})], \quad a \in U_t. \end{aligned} \quad (39)$$

Thus, stopping is evaluated by the expected prediction loss under the current conditional distribution of the label, while acquiring feature a is evaluated by the acquisition cost plus the expected prediction loss after observing feature a and then stopping. The ideal one-step policy is

$$a_t^* \in \arg \min_{a \in \mathcal{A}(S_t)} Q_1(x(m_t), a). \quad (40)$$

To make the stopping rule explicit, define the expected one-step loss reduction as

$$\Delta_t(a) \triangleq \mathbb{E}_{\mathbf{y}|x_{S_t}} [\ell(f_\phi(x(m_t)), \mathbf{y})] - \mathbb{E}_{\mathbf{x}_a, \mathbf{y}|x_{S_t}} [\ell(f_\phi(\mathbf{x}(m_{t+1})), \mathbf{y})]. \quad (41)$$

From (39), acquiring feature a is better than stopping immediately exactly when

$$\Delta_t(a) > \alpha c(a). \quad (42)$$

Thus, the myopic policy acquires the feature with the largest cost-adjusted expected loss reduction $\Delta_t(a) - \alpha c(a)$ if this quantity is positive, and otherwise selects $d+1$, the stopping action. Equivalently, it stops when $\Delta_t(a) \leq \alpha c(a)$ for every available feature $a \in U_t$, i.e., when no available feature has expected one-step loss reduction exceeding its cost penalty. Here, “myopic” refers to the planning rule used to choose the next action: it evaluates only the value of acquiring one more feature and then stopping. This is distinct from the maximum acquisition horizon k . A myopic method can still be run sequentially for up to k acquisitions by repeatedly applying the one-step rule, whereas NM-PPG optimizes a k -step truncated objective and therefore propagates learning signals through the remaining $k - t$ future acquisition decisions. Thus, k acts as a shared maximum rollout horizon, while the distinction between myopic and non-myopic methods is whether the action score itself reasons beyond one step. Equation (42) also shows that, for myopic methods, feature costs do not necessarily need to enter the acquisition-score training objective explicitly. In principle, one can train a model to estimate $\Delta_t(a)$ across relevant states and then compare this estimate against $\alpha c(a)$ only at inference. This is important for interpreting baselines such as DiFA, GDFS, and SEFA, which were introduced for uniform-cost hard-budget settings and therefore do not train cost-aware acquisition scores. The methods below differ mainly in how they approximate or learn the one-step score.

DiFA. DiFA [23] was originally proposed for the hard-budget setting. Following prior work on myopic AFA [24], we adapt it to (2) by using its learned acquisition scores together with an entropy-based stopping heuristic, so that the policy may stop before the horizon k . DiFA learns a differentiable approximation to the one-step acquisition rule. Let a_t denote the feature selected by the policy at the current mask, and let m_{t+1} be the mask after adding this feature. For the acquisition update, DiFA trains the policy so that the selected one-step successor mask has low prediction loss,

$$\min_{\theta} \mathbb{E}_{\mathbf{x}, \mathbf{y}} \mathbb{E}_{\pi_\theta} [\ell(f_\phi(\mathbf{x}(m_{t+1})), \mathbf{y})], \quad m_{t+1} = m_t + (1 - m_t) \odot \text{onehot}(a_t). \quad (43)$$

Since the current loss $\ell(f_\phi(\mathbf{x}(m_t)), \mathbf{y})$ is fixed with respect to the candidate action at step t , minimizing the one-step successor loss is equivalent to maximizing the empirical loss decrease $\ell(f_\phi(\mathbf{x}(m_t)), \mathbf{y}) - \ell(f_\phi(\mathbf{x}(m_{t+1})), \mathbf{y})$. DiFA uses a straight-through Gumbel-Softmax acquisition during training: the forward pass uses a hard one-feature acquisition, while the backward pass uses the soft relaxation to propagate gradients to the policy. However, DiFA does not learn an estimate of the expected one-step loss reduction; it only learns which action is expected to produce a useful one-step successor, not the numerical value of the reduction. Therefore, it cannot directly apply

the cost-adjusted expectation-based stopping rule in (42), which requires comparing an expected reduction $\Delta_t(a)$ to the feature-cost penalty $\alpha c(a)$. At inference, it greedily acquires the highest-scoring available feature until the predictive label entropy of the masked predictor falls below the threshold α , or until the horizon k is reached. Entropy-threshold stopping has also been considered in prior AFA work [24]. This stopping rule assumes uniform feature costs, which is consistent with the hard-budget setting for which DiFA was originally introduced, where each feature has unit cost. Key hyperparameters are the entropy threshold α , the horizon k , the Gumbel temperature schedule $(\tau_{\text{start}}, \tau_{\text{end}})$, the policy and predictor learning rates, and architecture hyperparameters of the policy and predictor neural networks.

GDFS. GDFS [22] was also originally proposed for the uniform-cost hard-budget setting. We adapt it to the standard AFA objective in (2) by using the learned acquisition scores with the same entropy-threshold stopping rule as for DiFA. GDFS also targets the same myopic loss-reduction principle, but uses a fully soft differentiable acquisition during training. At step t , it samples a relaxed acquisition $\tilde{a}_t \in \Delta^d$ from the policy over currently available features and constructs a soft next mask

$$\tilde{m}_{t+1} = m_t + (1 - m_t) \odot \tilde{a}_t, \quad (44)$$

and optimizes the one-step successor prediction loss

$$\min_{\theta} \mathbb{E}_{\mathbf{x}, \mathbf{y}} \mathbb{E}_{\pi_{\theta}} [\ell(f_{\phi}(\mathbf{x}(\tilde{m}_{t+1})), \mathbf{y})]. \quad (45)$$

Thus, as in (39), the learned policy is encouraged to choose features that most improve the terminal prediction after one additional acquisition. Unlike DiFA, the predictor in GDFS is trained on fractional masks induced by the relaxed acquisition. Like DiFA, however, GDFS does not learn an expected one-step loss reduction; it learns acquisition logits for choosing a high-improvement action, not the numerical value of the reduction. Therefore, the cost-adjusted one-step stopping rule in (42) is not directly available, since that rule requires comparing an expected reduction $\Delta_t(a)$ to the feature-cost penalty $\alpha c(a)$. At test time, the learned policy is made deterministic by selecting the largest available feature logit, while stopping is handled by predicting once the predictive label entropy is below α , or once the horizon k is reached. As for DiFA, this entropy-threshold stopping rule assumes uniform feature costs, matching the original hard-budget setting where each feature has unit cost. Key hyperparameters are α , the horizon k , the Gumbel temperature and learning-rate schedules, the policy/predictor learning rates, and architecture hyperparameters of the policy and predictor neural networks.

DIME. DIME [24] makes the one-step value approximation explicit. Let $m_{t+1} = m_t + (1 - m_t) \odot \text{onehot}(a_t)$. It trains a value network $q_{\xi}(x(m_t), a_t)$ to predict the empirical one-step loss decrease from acquiring feature a_t :

$$q_{\xi}(\mathbf{x}(m_t), a_t) \approx \hat{g}_{a_t}(\mathbf{x}(m_t)) \triangleq \ell(f_{\phi}(\mathbf{x}(m_t)), \mathbf{y}) - \ell(f_{\phi}(\mathbf{x}(m_{t+1})), \mathbf{y}). \quad (46)$$

Training minimizes a squared Bellman-style one-step regression loss,

$$\min_{\xi} \mathbb{E}_{\mathbf{x}, \mathbf{y}} \mathbb{E}_{\pi_{\theta}} \left[(q_{\xi}(\mathbf{x}(m_t), a_t) - \hat{g}_{a_t}(\mathbf{x}(m_t)))^2 \right], \quad (47)$$

while the predictor is trained on the masks encountered during the same acquisition process. Since DIME explicitly estimates the gain, one could directly implement the stopping rule in (42) by acquiring $\arg \max_{a \in U_t} (q_{\xi}(x(m_t), a) - \alpha c(a))$ when this maximum is positive, and stopping otherwise. The original DIME paper instead uses a cost-normalized rule: it acquires the feature with largest value of $q_{\xi}(x(m_t), a)/c(a)$, and stops when this ratio is below the threshold α . This is closely related to the one-step values in (39), but uses a gain-per-cost threshold rather than the additive cost-adjusted rule above. Key hyperparameters are α , the horizon k , the ϵ -greedy exploration schedule, the value and predictor learning rates, and architecture hyperparameters of the value and predictor neural networks.

C.1.2 Non-Myopic Baselines

The remaining baselines are non-myopic in the sense that they attempt to account for the effect of current acquisitions on later decisions, either through explicit lookahead, latent-variable acquisition scoring, or RL over the sequential acquisition process. AACO and SEFA represent a different approach from directly optimizing long-term cost minimization in the AFA-POMDP. They exploit the structure of AFA by recognizing that non-myopic acquisition requires reasoning about feature

groups that are jointly informative about the label, even if the individual features in the group are not immediately useful on their own. Their acquisition rules therefore try to identify such jointly informative groups and then acquire one feature from the selected group. This can make the methods more stable than generic RL, but it also introduces bias relative to the full AFA-POMDP: the joint informativeness is assessed by a heuristic, non-adaptive criterion conditioned on the currently observed features, rather than by optimizing over the full adaptive future policy that can react to the values of newly acquired features.

AACO. AACO [12] is a non-myopic AFA baseline that performs lookahead through candidate subsets rather than through an explicit RL policy. For a current partial observation, AACO first finds nearby training examples under the currently observed features. It then samples many candidate subsets of remaining actions, fills the candidate-acquired features using the corresponding values from the local neighbors, and evaluates the masked predictor loss for each candidate subset. The selected subset minimizes a cost-regularized objective of the form estimated prediction loss plus α times acquisition cost; the method then acquires one feature from that selected subset and repeats. Intuitively, AACO solves a cost-sensitive non-myopic, but static and non-adaptive, feature-selection problem conditioned on the features acquired so far. The AACO paper proves that this objective is a lower bound on the optimal value function in the AFA-POMDP. This lower-bound interpretation is useful, but it also shows that AACO optimizes a surrogate rather than exact long-term cost minimization in the AFA-POMDP, and is therefore biased relative to the full sequential problem. Because this acquisition rule is non-parametric, AACO has no separate parametric acquisition-policy training stage. In our implementation, however, we still roll out the AACO acquisition rule on the training data and use the visited masks to further train the masked predictor. This aligns the predictor with the policy-induced state distribution and performed better than using only the predictor pretrained on random masks. Key hyperparameters are the trade-off parameter α , the maximum rollout horizon k , the number of nearest neighbors, the number of candidate subsets, and architecture hyperparameters of the masked predictor.

SEFA. SEFA [32] was also originally proposed for the uniform-cost hard-budget setting. Its sensitivity-based acquisition score is therefore not cost-adjusted and does not natively support non-uniform feature costs. SEFA trains a stochastic encoding model for partially observed inputs. The model maps each observed masked input to a latent distribution, predicts the label from Monte Carlo latent samples, and is trained with a negative log-likelihood term plus a KL-style information-bottleneck penalty. At inference, SEFA computes acquisition scores from the sensitivity of the predictive distribution to each feature’s latent representation, then greedily acquires the highest-scoring available feature. To adapt SEFA to (2), we use the same entropy-threshold stopping heuristic as for DiFA and GDFS: the method stops once normalized predictive entropy falls below the threshold α , or once the horizon k is reached. Key hyperparameters are α , the horizon k , the latent dimension, the bottleneck weight β , the numbers of Monte Carlo samples used for training, prediction, and acquisition scoring, and architecture hyperparameters of the encoder and predictor neural networks.

GSMRL. GSMRL [26] is a model-based non-myopic RL baseline targeting the standard AFA objective in (2). It augments the acquisition policy with a learned ACFlow-style surrogate model that estimates both unobserved feature distributions and label probabilities from the current partial observation. The policy is optimized with PPO over a discrete action space containing all feature acquisitions and STOP. Appendix F.1 gives the formal AFA-POMDP instantiation of (2), with immediate costs specified in (60): acquiring feature a incurs cost $\alpha c(a)$, while stopping incurs the prediction loss at the stopping mask. GSMRL additionally uses model-based information-gain terms from the surrogate model to shape acquisition decisions. The masked predictor is also updated on hard masks visited by the policy. Key hyperparameters are α , the horizon k , PPO parameters such as the clipping parameter, number of PPO epochs, minibatch size, discount factor γ , critic weight, and entropy coefficient, as well as ACFlow pretraining hyperparameters and architecture hyperparameters of the policy, critic, predictor, and ACFlow neural networks.

OL. OL [30] is a model-free non-myopic RL baseline based on DQN. It was originally proposed for the hard-budget setting. We adapt OL to the standard AFA objective in (2) by modifying the reward according to the AFA-POMDP costs in (60): acquiring feature a incurs cost $\alpha c(a)$, while stopping incurs the prediction loss of the P -branch at the current mask. The method uses a joint P/Q network: the P -branch predicts the label from the current masked input, while the Q -branch predicts action values for feature acquisitions and stopping, using detached hidden activations from the P -branch as side information. During training, transitions are stored in a replay buffer and a

Table 1: Use of the horizon k in all methods.

Method	Use of k during training	Use of k during inference
NM-PPG	Truncation horizon for the ST rollout objective in Alg. 2.	Maximum number of feature acquisitions before forced prediction.
DiFA	Caps sequential training rollouts; each update optimizes a one-step successor loss.	Maximum number of feature acquisitions before forced prediction.
GDFS	Caps sequential training rollouts; each update optimizes a one-step soft successor loss.	Maximum number of feature acquisitions before forced prediction.
DIME	Caps rollouts used to collect states and one-step gain targets for value regression.	Maximum number of feature acquisitions before forced prediction.
AACO	Caps training-data rollouts used only to collect masks for predictor alignment.	Maximum number of feature acquisitions before forced prediction.
SEFA	Not used in the gradient training loss; used only for validation acquisition AUC/model selection.	Maximum number of feature acquisitions before forced prediction.
GSMRL	PPO rollout horizon for collecting transitions and computing policy/value updates.	Maximum number of feature acquisitions before forced prediction.
OL	DQN episode horizon for collecting replay transitions and training P/Q networks.	Maximum number of feature acquisitions before forced prediction.

Table 2: Summary of benchmark datasets. For Cube-NM we use $n_c = 5$.

Dataset	Type	Train	Validation	Test	# Features	# Classes	Imbalanced	Non-uniform cost
Cube-NM ($\sigma = 0.1$)	Synthetic	7,000	1,500	1,500	55	8	No	Yes
Cube-NM ($\sigma = 0.2$)	Synthetic	7,000	1,500	1,500	55	8	No	Yes
Syn1	Synthetic	60,000	10,000	10,000	11	2	No	No
Syn3	Synthetic	60,000	10,000	10,000	11	2	No	No
Connect4	Real-world tabular	47,290	10,133	10,134	42	3	Yes	No
Splice	Real-world tabular	2,233	478	479	60	3	No	No
EngineFaultDB	Real-world tabular	39,200	8,400	8,399	14	4	No	No
Metabric	Real-world medical	1,329	285	284	662	6	No	No
Mortality	Real-world medical	9,409	2,016	2,017	26	2	Yes	Yes
Diabetes	Real-world medical	64,443	13,809	13,810	33	3	Yes	Yes
MNIST	Real-world image	50,000	10,000	10,000	784	10	No	No
Fashion-MNIST	Real-world image	50,000	10,000	10,000	784	10	No	No

target network is updated by Polyak averaging. At inference, OL greedily selects the largest masked Q-value until STOP or the horizon. Key hyperparameters are α , the horizon k , discount factor γ , ϵ -greedy exploration schedule, replay-buffer size and minimum replay size, Q-minibatch size, number of Q updates per episode, target-update rate, and architecture hyperparameters of the P/Q neural network.

C.1.3 Use of the horizon k

Table 1 summarizes how k is used for all methods. In all cases, k is a maximum acquisition horizon or rollout cap, not necessarily the planning depth of the method. In particular, the myopic baselines can be trained and evaluated over trajectories of length up to k , but their action scores remain one-step scores.

C.2 Datasets

This subsection provides additional details for each benchmark dataset used in our experiments. Table 2 provides summary information about each dataset. The # Features column reports the number of acquisition feature groups used by the AFA policies. Some processed features, such as one-hot encoded categorical variables, are treated as a single acquisition because they effectively correspond to the same underlying feature; this avoids forcing the policy to learn to acquire all components of such a group separately. We specify below how feature groups are formed for each dataset.

Cube-NM. Cube-NM [31] is a synthetic AFA dataset designed to isolate the benefit of non-myopic acquisition. Each instance has a latent context that selects which one of several feature blocks

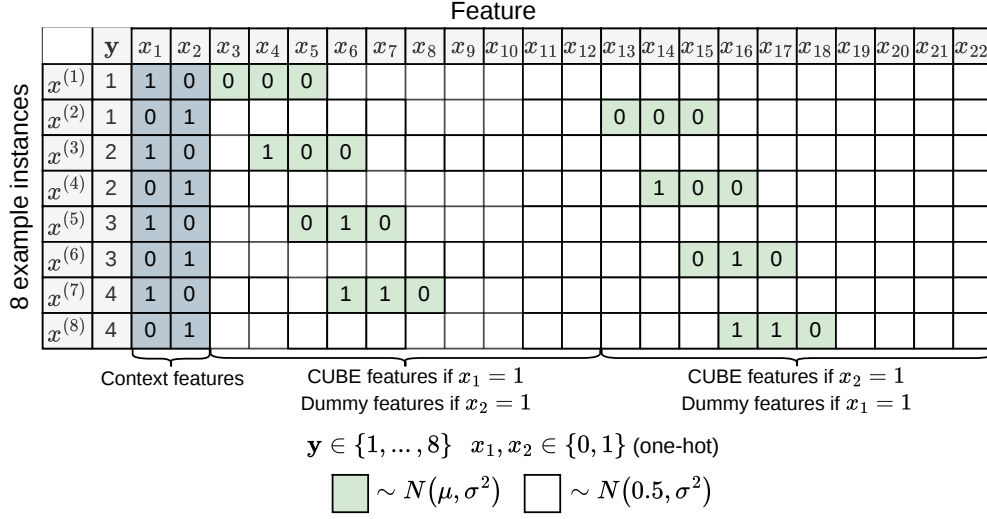


Figure 2: Illustration of the Cube-NM context mechanism for $n_c = 2$. The first two features x_1, x_2 form the one-hot context. If $x_1 = 1$, features x_3, \dots, x_{12} are the CUBE block and x_{13}, \dots, x_{22} are dummy features; if $x_2 = 1$, the roles are reversed. Blue entries are sampled from $\mathcal{N}(\mu, \sigma^2)$, where μ is the corresponding coordinate of the class prototype p_y for label y . White entries are sampled from the dummy distribution $\mathcal{N}(0.5, \sigma^2)$. The experiments use $n_c = 5$ and $\sigma \in \{0.1, 0.2\}$.

contains label information; the context features reveal this block identity but do not directly reveal the label. We use x_i to denote the scalar value of feature i . Formally, with n_c possible contexts, the first n_c features, x_1, \dots, x_{n_c} , are one-hot context indicators. The remaining features are split into n_c feature blocks of size 10: the block for context j consists of $x_{n_c+10(j-1)+1}, \dots, x_{n_c+10j}$. In Figure 2, we illustrate this construction for $n_c = 2$: x_1, x_2 are context features, the first candidate block is x_3, \dots, x_{12} , and the second candidate block is x_{13}, \dots, x_{22} .

An instance is generated by sampling a label $y \in \{1, \dots, 8\}$ and an active context $r \in \{1, \dots, n_c\}$. The context features are set to $x_r = 1$ and $x_j = 0$ for $j \leq n_c, j \neq r$. Because r is sampled independently of y , these context features do not directly predict the label; they only reveal which feature block of size 10 contains label information.

The label controls the mean of the active block through a class prototype p_y . Here $p_y \in \mathbb{R}^{10}$ is not an observed feature; it is the length-10 mean vector used to generate the informative block for class y . To define it, set $q = y - 1$, write q in binary as (q_0, q_1, q_2) , initialize all ten entries of p_y to 0.5, and replace entries $q + 1, q + 2, q + 3$ by (q_0, q_1, q_2) . For example, if $y = 6$, then $q = 5$, the bits are $(1, 0, 1)$, and p_y has entries 1, 0, 1 in positions 6, 7, 8 and 0.5 elsewhere.

Finally, features are sampled. If r is the active context, then for local coordinate $\ell = 1, \dots, 10$, the feature $x_{n_c+10(r-1)+\ell}$ in the active block is sampled from $\mathcal{N}(p_y^{(\ell)}, \sigma^2)$. For every inactive context $j \neq r$, the dummy-block feature $x_{n_c+10(j-1)+\ell}$ is sampled from $\mathcal{N}(0.5, \sigma^2)$. Therefore, only the active block has a label-dependent mean pattern; all dummy blocks are centered at 0.5 and carry no label information. In Figure 2, this means that if $x_1 = 1$, then x_3, \dots, x_{12} are sampled from the class prototype and x_{13}, \dots, x_{22} are dummy features; if $x_2 = 1$, the roles are reversed.

In our experiments we use $n_c = 5$, noise levels $\sigma \in \{0.1, 0.2\}$, context-feature cost 0.2, and non-context feature cost 1, giving $5 + 5 \cdot 10 = 55$ processed features. This creates the non-myopic structure: a context feature can have little immediate predictive value, but it determines which expensive block should be queried next. The paper that introduced Cube-NM proves that, in the noiseless setting, non-myopic selection can require substantially fewer acquisitions than a myopic policy:

Theorem 3 (Informal Cube-NM result [31]). *Consider the noiseless Cube-NM dataset with n_c contexts and $\sigma = 0$, so that 100% prediction accuracy is achievable. Then a myopic policy requires, in expectation over instances, $13(2n_c + 1)/16$ feature acquisitions to achieve 100% accuracy. In*

contrast, there exists an optimal non-myopic policy that achieves 100% accuracy after acquiring only $\mathbf{1}\{n_c \geq 2\} + 9/4$ features in expectation.

The exact constants in Theorem 3 assume that the context is acquired as a single categorical feature, equivalently as one acquisition group containing the one-hot context indicators. In our experiments, we do not group these context indicators, making the dataset slightly more challenging. The same qualitative non-myopic structure applies, but the exact expected acquisition counts differ.

Theorem 3 also illustrates how the advantage of non-myopic selection depends on the number of contexts. As n_c increases, the myopic acquisition cost grows linearly in n_c , while the non-myopic policy remains constant after $n_c \geq 2$. This reflects the general principle that non-myopic AFA is most useful when early acquisitions reveal which later acquisitions are valuable; see Appendix G for a more detailed discussion.

Syn1. Syn1 is one of the synthetic datasets used in previous AFA work to evaluate non-myopic acquisition methods [32]. These datasets are useful because they are constructed so that the optimal acquisition order is known. Each instance consists of 11 independent standard-normal features x_1, \dots, x_{11} , with x_{11} acting as a context feature that determines which feature interaction generates the label. If $x_{11} < 0$, the label probability is determined by the interaction $\ell_1 = 4x_1x_2$, while if $x_{11} \geq 0$, it is determined by the quadratic block $\ell_2 = 1.2 \sum_{j=3}^6 x_j^2 - 4.2$. In both cases, $p(y = 1) = 1/(1 + \exp(\ell))$, where ℓ is the selected logit. Thus, x_{11} does not directly define the label by itself; instead, it indicates whether the useful information is contained in the pair (x_1, x_2) or in the block x_3, \dots, x_6 . This makes Syn1 a controlled test of whether an AFA method can acquire a context feature before selecting the features that are predictive under that context.

Syn3. Syn3 is another synthetic dataset used in previous AFA work to evaluate non-myopic acquisition methods [32]. It uses the same 11-feature construction and the same context variable x_{11} , but switches between two higher-order feature blocks. If $x_{11} < 0$, the label is generated from the quadratic block $\ell_2 = 1.2 \sum_{j=3}^6 x_j^2 - 4.2$. If $x_{11} \geq 0$, it is generated from the nonlinear block $\ell_3 = -10 \sin(0.2x_7) + |x_8| + x_9 + \exp(-x_{10}) - 2.4$. As in Syn1, $p(y = 1) = 1/(1 + \exp(\ell))$ for the selected logit. Syn3 is therefore a harder context-dependent benchmark with a known optimal acquisition order: the policy must first identify which branch applies, and then acquire features from either x_3, \dots, x_6 or x_7, \dots, x_{10} . All Syn1 and Syn3 features have unit acquisition cost.

Connect4. Connect4 [44] is a board-state classification dataset. The prediction task is to classify the eventual game outcome, i.e., loss, draw, or win, from the current Connect Four board. The board has 42 cells, each taking one of three values: empty, player x , or player o . We one-hot encode each cell, giving 126 processed binary features, and treat each board cell as one acquisition group so that acquiring a cell reveals its full categorical state. This is useful for AFA because only a subset of board positions may be needed to determine the outcome, mimicking decision settings where an agent should inspect only the most informative parts of a structured state.

Splice. Splice [45] is a DNA splice-junction classification dataset. The prediction task is to classify a length-60 DNA sequence as a non-splice example, an exon-intron junction, or an intron-exon junction. We one-hot encode the nucleotide at each sequence position, yielding 480 processed binary features, and treat each sequence position as one acquisition group. This is relevant for AFA because biological sequence assays can be costly, and the predictive signal may be concentrated in a small subset of positions around the junction.

EngineFaultDB. EngineFaultDB [46] is a real-world tabular engine fault diagnosis dataset. The prediction task is to identify one of four engine fault classes from 14 numeric sensor measurements. We normalize the measurements using training-set statistics and treat each sensor value as one acquisition. This is a natural AFA setting because diagnostic systems may be able to query additional sensors or tests sequentially, but each measurement can consume time, energy, or hardware resources.

Metabric. Metabric [47, 48] is a real-world medical breast cancer dataset. The prediction task is to classify the PAM50 plus claudin-low molecular subtype, giving six classes after removing invalid labels. We use the molecular feature block from the processed METABRIC table, resulting in 662 gene-expression and mutation features. Expression features are winsorized and standardized using training-set statistics, and each molecular measurement is treated as one acquisition. This is important for AFA because molecular profiling can be expensive, and an adaptive policy may reduce the number of assays needed for accurate subtype prediction.

Mortality. Mortality is derived from the National Health and Nutrition Examination Survey (NHANES) [49], and was processed into an outpatient mortality benchmark in [54]. The prediction task is binary 10-year mortality prediction from demographic variables, laboratory measurements, examination results, and questionnaire-derived variables. The raw clinical variables are expanded into 118 processed columns, including continuous measurements, binary indicators, missingness indicators, test-status indicators such as unacceptable or test-not-done flags, and one-hot encodings for categorical measurements. In the AFA setup, acquisition is defined at the level of the underlying clinical variable or measurement panel: acquiring a group reveals all processed columns derived from that variable or panel. For example, a laboratory measurement group can include the measured value together with its missingness and test-status indicators, and categorical urine-test groups include all corresponding one-hot indicators. This gives 26 acquisition groups with non-uniform costs. The feature costs follow the CoAI setup, where costs were assigned to reflect monetary burden and patient inconvenience [54]. We standardize numeric features and handle missing values using training-set statistics. This is an important AFA benchmark because clinical risk assessment often involves deciding which patient information or lab tests are worth collecting before making a prediction.

Diabetes. Diabetes is derived from NHANES [49] in the OL paper [30], a prior AFA work that used this dataset as a benchmark. The feature set contains demographic variables, laboratory results, examination measurements, and questionnaire answers, including variables such as age, gender, ethnicity, total cholesterol, triglycerides, weight, height, smoking, alcohol use, and sleep habits. The prediction task is three-class diabetes status prediction, where fasting glucose values define the classes normal, pre-diabetes, and diabetes according to standard threshold values. The original benchmark contains 92,062 samples and 45 processed feature columns. In our AFA setup, one-hot encoded categorical variables are treated as acquisition groups, so acquiring the original categorical variable reveals all of its one-hot indicators; this gives 33 acquisition groups. We impute missing values using training-set statistics, winsorize and standardize continuous features, and keep binary features unchanged. The non-uniform feature costs follow the OL setup, where a medical expert assigned costs based on financial burden, patient privacy, and patient inconvenience. This dataset is relevant for AFA because diabetes screening combines cheap background variables with potentially more costly clinical measurements, making adaptive test selection practically meaningful.

MNIST. MNIST [50] is a 10-class handwritten digit recognition dataset. The prediction task is to classify the digit identity from a 28×28 grayscale image. As for Fashion-MNIST, we flatten each image into 784 normalized pixel features and treat pixels as individually acquirable features. This provides a canonical image benchmark for evaluating whether AFA methods can classify accurately while observing only a subset of pixels. The AFA motivation is again fast visual decision-making: in applications such as real-time detection or embedded recognition, acquiring or processing fewer image locations can reduce latency and computation [55].

Fashion-MNIST. Fashion-MNIST [51] is a 10-class image classification dataset of clothing items. The prediction task is to classify the object category from a 28×28 grayscale image. We flatten each image into 784 normalized pixel features and treat each pixel as one acquisition. In the AFA setting, this tests whether a method can identify an object while observing only a subset of pixels. This is motivated by real-time visual recognition settings, where fast inference can require focusing computation on informative image regions rather than processing every pixel, as in classical cascaded detection systems [55].

C.3 Hyperparameter Details

Tuning of α . For all methods, we tune the trade-off parameter α . These values are chosen so that the resulting curves cover a reasonable range of acquisition costs and predictive performance. In particular, we avoid grids where most settings collapse to the same point, for example several values that all attain essentially the same best predictive performance while using different costs, or several values that all lead to zero acquisition. Thus, each reported curve is intended to show the relevant cost–performance trade-off for that method on that dataset (in Figure 1).

NM-PPG Hyperparameters. The main paper specifies the key NM-PPG hyperparameters. The remaining NM-PPG choices are standard across datasets, except that we tune NM-PPG hyperparameters on the validation split when required. The predictor is trained with cross-entropy loss, using class weights for imbalanced datasets. The policy and predictor are optimized with Adam [56]. Before policy optimization, the predictor is warm-started on randomly sampled masks; during policy

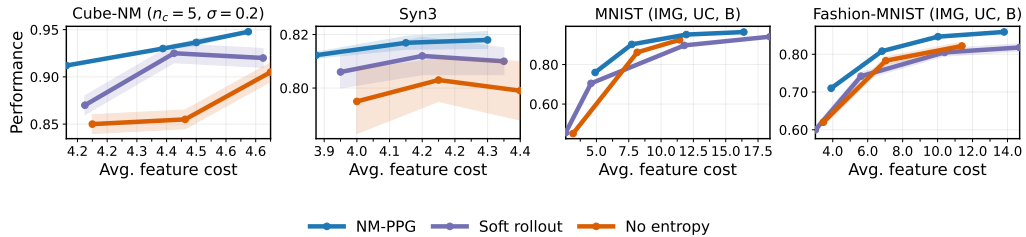


Figure 3: Ablation study comparing NM-PPG with two variants: a soft-rollout variant that optimizes the relaxed objective in (8) directly, and a no-entropy variant with $\lambda_{\text{ent}} = 0$. Performance is measured by accuracy for balanced datasets and F1-score for imbalanced datasets.

optimization, it is refined on rollout-visited masks through L_{pred} , as described in Appendix B. Model selection uses the deterministic validation loss induced by the current policy and predictor.

Baseline Hyperparameters. For baseline methods, we use the hyperparameters and implementation details recommended in the original papers as a starting point. Appendix C.1 lists the key hyperparameters for each baseline. We refer to the original papers and implementations of these baselines for the corresponding hyperparameter choices. We then tune from these starting points when required for different datasets. All such tuning is performed using training and validation data only, with the same evaluation protocol applied to all methods.

Shared Architecture, Losses, and Model Selection. Across methods, we use the same train/validation/test splits, preprocessing pipeline, feature groups, feature costs, primary metric, and label loss for each dataset. Unless otherwise required by a baseline implementation, neural predictors are trained with cross-entropy loss, using class weights for imbalanced datasets, and optimized with Adam using the method-specific learning rates. We use consistent neural architectures across methods whenever the method permits it. The masked predictor and the fully observed predictor are both two-hidden-layer MLPs with ReLU activations and dropout 0.3 after each hidden layer. The hidden width is 256 for Cube-NM, Connect4, EngineFaultDB, Splice, MNIST, and Fashion-MNIST, and 128 for Metabarc, Mortality, and Diabetes. Policy networks use two-hidden-layer ReLU MLPs without dropout, with the same dataset-dependent hidden widths for NM-PPG. For GSMRL, which uses PPO, the critic/value network uses the same two-hidden-layer ReLU architecture as the corresponding policy network. For OL, we use the original shared P/Q architecture with two hidden layers, the same dataset-dependent hidden width as above, and dropout 0.1 in the predictor branch during training. For SEFA, we use two hidden layers of width 256 for both the encoder and predictor, with batch normalization as in the original method. Method-specific auxiliary models, such as the ACFlow-style surrogate used by GSMRL, use the architecture prescribed by the corresponding baseline implementation. Model selection is performed only on the validation split, and test results are computed only after this validation-based selection.

C.4 Ablation Studies

The ablation study isolates two key design choices in NM-PPG. First, to evaluate the ST rollout procedure from Section 3.3, we compare NM-PPG to a soft-rollout variant that optimizes the fully relaxed objective in (8) directly instead of the ST objective in (10). Second, to evaluate entropy regularization from Section 3.4, we compare against a variant with $\lambda_{\text{ent}} = 0$. Figure 3 shows that both components are useful: the ST rollout improves alignment with the discrete deployment policy, while entropy regularization helps maintain exploration during policy optimization.

C.5 Acquisition Paths

Figures 4–8 visualize acquisition trajectories for NM-PPG and representative baselines. The synthetic plots compare against GDFS, GSMRL, and SEFA, while the clinical real-world plot compares against GDFS, GSMRL, and AACO. Each panel is a feature-by-step heatmap: the x -axis gives the acquisition step, the y -axis gives the feature, feature group, or STOP action, and the color indicates the percentage of test instances for which the method selects that row at that step. For synthetic datasets, each row

shows a context-defined subset of test instances. For readability, each row shows the most frequently acquired feature groups across the displayed methods and the first eight acquisition steps. The plots are intended to show not only how many features each method acquires, but also whether the learned policy uses early acquisitions as context for later decisions.

Cube-NM. Figures 4 and 5 show the two Cube-NM variants with $n_c = 5$. The first five features are context features: they are weak predictors by themselves, but they identify which later feature block is informative for the current instance. NM-PPG consistently acquires context features early and then follows up with context-dependent feature acquisitions, which is the intended non-myopic behavior. GDFS behaves differently. For $\sigma = 0.1$, it largely skips the context features and directly acquires features that look locally predictive, as expected for a myopic method. For $\sigma = 0.2$, GDFS sometimes acquires context features, but its later acquisitions do not cleanly follow the context; this is consistent with the noisier setting making context features appear locally useful without giving GDFS a mechanism to plan the follow-up sequence. GSMRL can sometimes recover a similar context-first behavior, but tends to use more acquisitions, while SEFA is more diffuse and less consistently aligned with the context structure.

Syn1. Figure 6 shows that NM-PPG first acquires x_{11} , the context feature, for both $x_{11} < 0$ and $x_{11} \geq 0$. It then branches to different feature groups depending on the context value, for example primarily selecting x_1 and x_2 in one branch and x_3 and x_4 in the other. GDFS instead tends to select the same locally useful features before observing the context, so its policy is less instance-adaptive. GSMRL also often discovers the context-first policy on Syn1, while SEFA partially uses x_{11} but produces a less concentrated acquisition pattern.

Syn3. Figure 7 shows a similar pattern on Syn3. NM-PPG again uses x_{11} as the first acquisition and then changes the later feature sequence depending on whether $x_{11} < 0$ or $x_{11} \geq 0$. In contrast, GDFS typically starts with a non-context feature and only acquires x_{11} later, if at all, which means the context cannot guide the earliest acquisition decisions. GSMRL also finds an early-context policy on this dataset, whereas SEFA is less stable and often starts from a locally predictive feature rather than the context feature.

NHANES Mortality. The first row of Figure 8 shows NHANES Mortality. The main groups selected by NM-PPG are x_{17} , serum protein, followed by x_{12} , potassium. GDFS instead starts from x_{19} , sodium, and usually stops after this single acquisition. Thus, NM-PPG learns a two-step biochemical screening policy, while the myopic baseline prefers a single locally predictive electrolyte measurement. GSMRL is closer to NM-PPG and often uses the same early sequence, although with additional later acquisitions, while AACO is more variable across instances.

NHANES Diabetes. The second row of Figure 8 shows NHANES Diabetes. Here x_2 is age (RIDAGEYR), x_{21} is triglycerides (LBXTR), and x_{23} is LDL cholesterol (LBDLDL). NM-PPG first acquires age and then acquires triglycerides only for a subset of instances. GDFS instead acquires triglycerides immediately and then usually stops, which is a myopic policy because it pays for the expensive laboratory feature before using cheap demographic context. GSMRL also discovers the age-then-triglycerides pattern, whereas AACO more often starts directly from triglycerides or LDL cholesterol. This provides a real-world example where NM-PPG and GSMRL identify a context-first policy that GDFS does not recover.

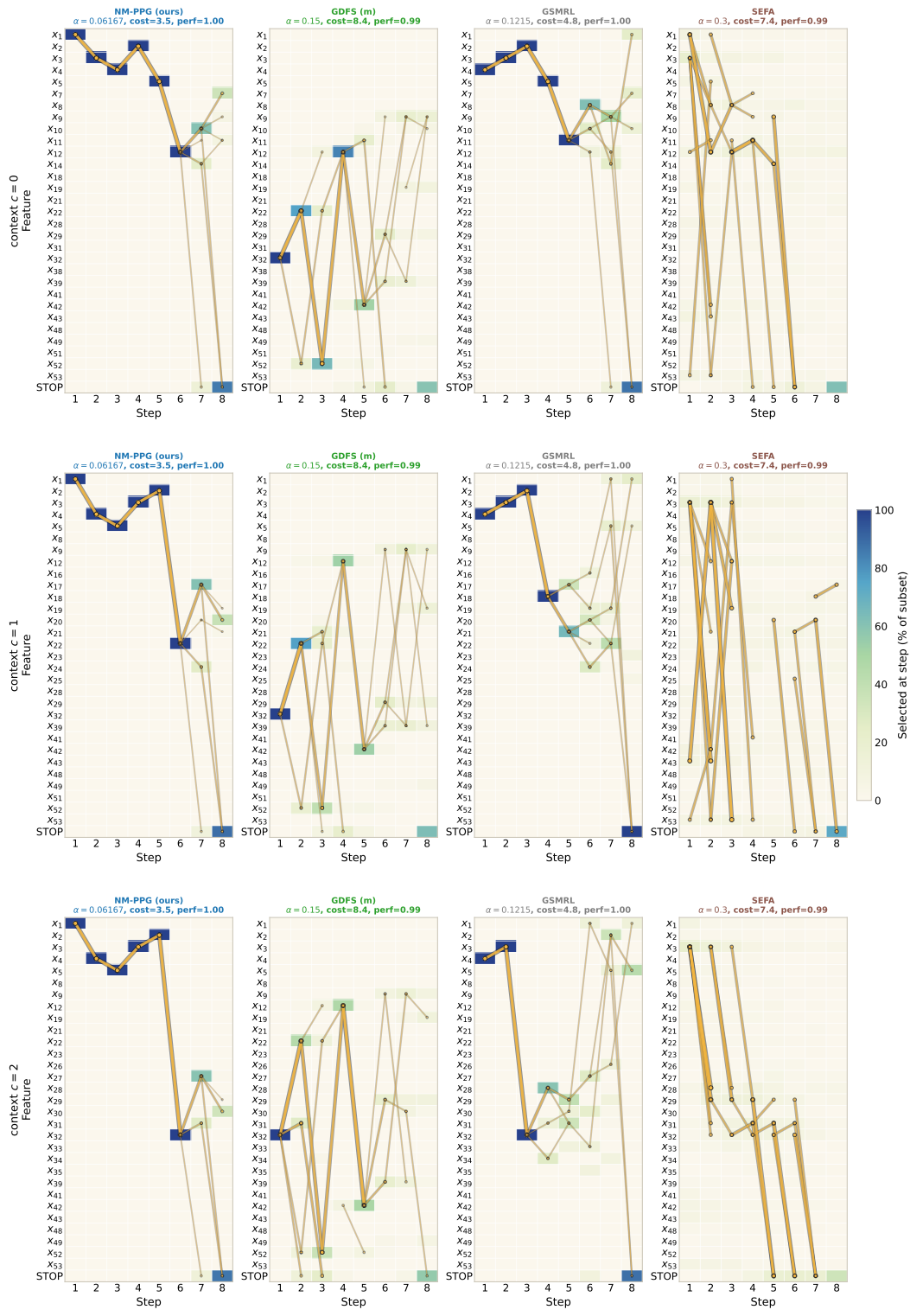


Figure 4: Acquisition trajectories on Cube-NM with $n_c = 5$ and $\sigma = 0.1$. Rows show three different context values. NM-PPG is compared with GDFS, GSMRL, and SEFA using feature-by-step acquisition-frequency heatmaps.

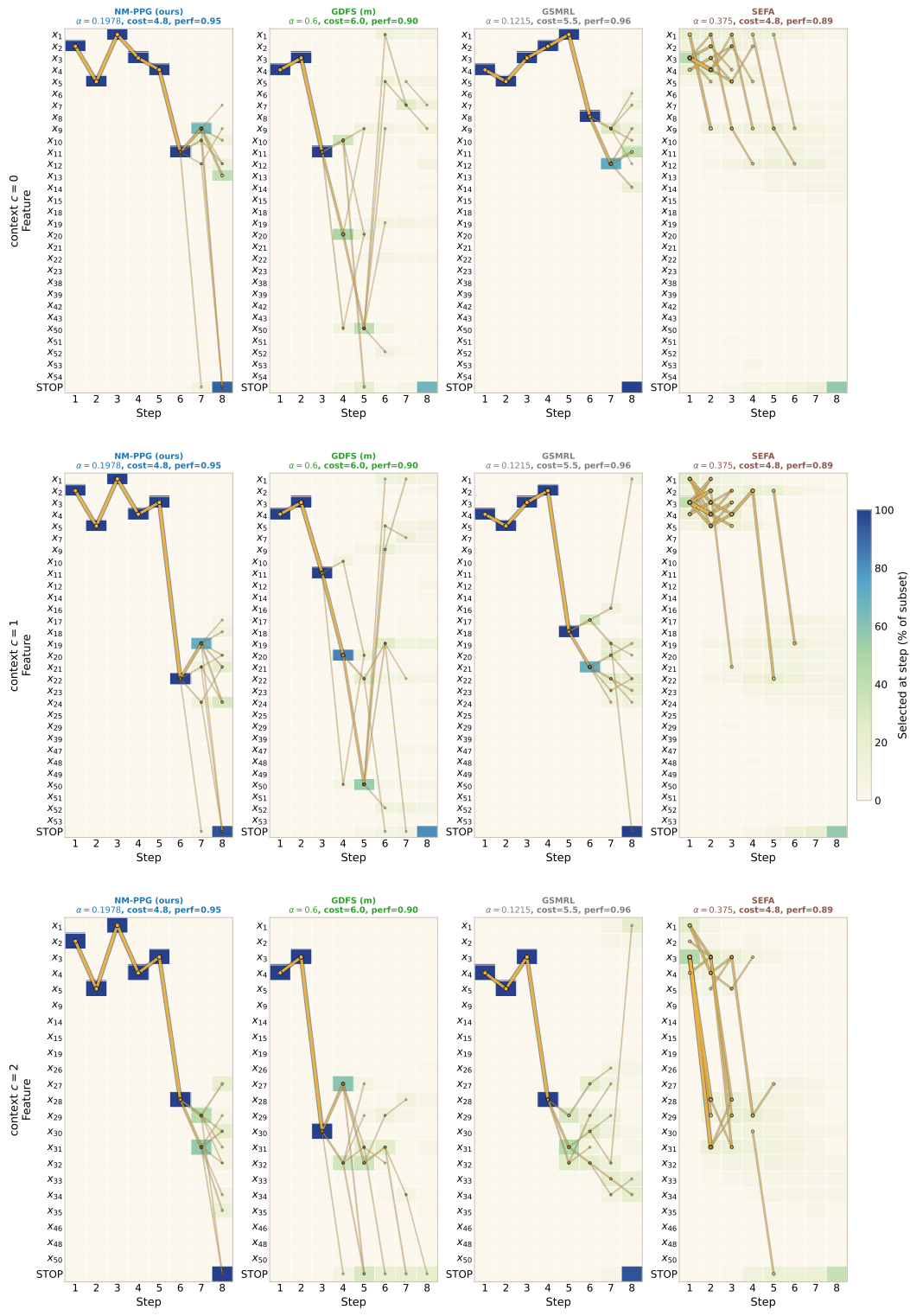


Figure 5: Acquisition trajectories on Cube-NM with $n_c = 5$ and $\sigma = 0.2$. Rows show three different context values. NM-PPG is compared with GDFS, GSMRL, and SEFA using feature-by-step acquisition-frequency heatmaps.

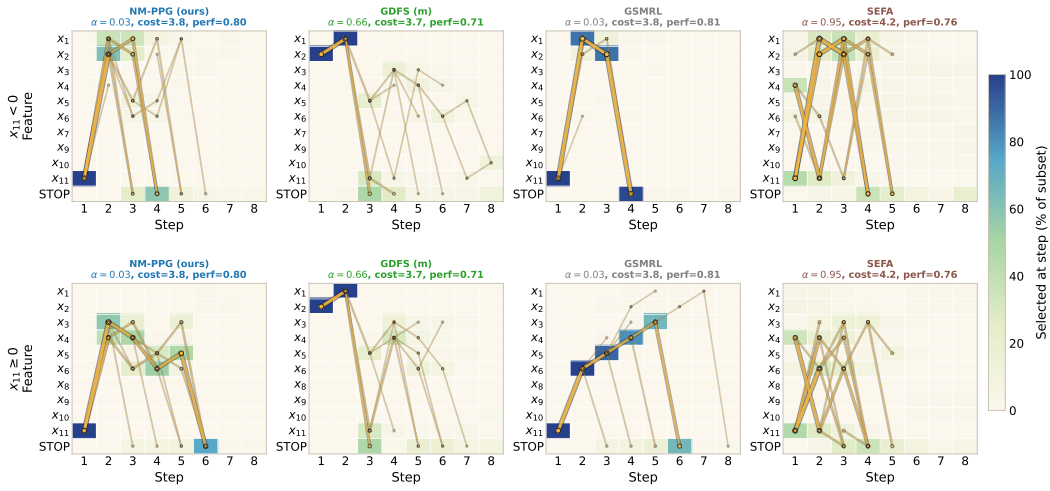


Figure 6: Acquisition trajectories on Syn1. Rows show instances with $x_{11} < 0$ and instances with $x_{11} \geq 0$. NM-PPG is compared with GDFS, GSMRL, and SEFA using feature-by-step acquisition-frequency heatmaps.

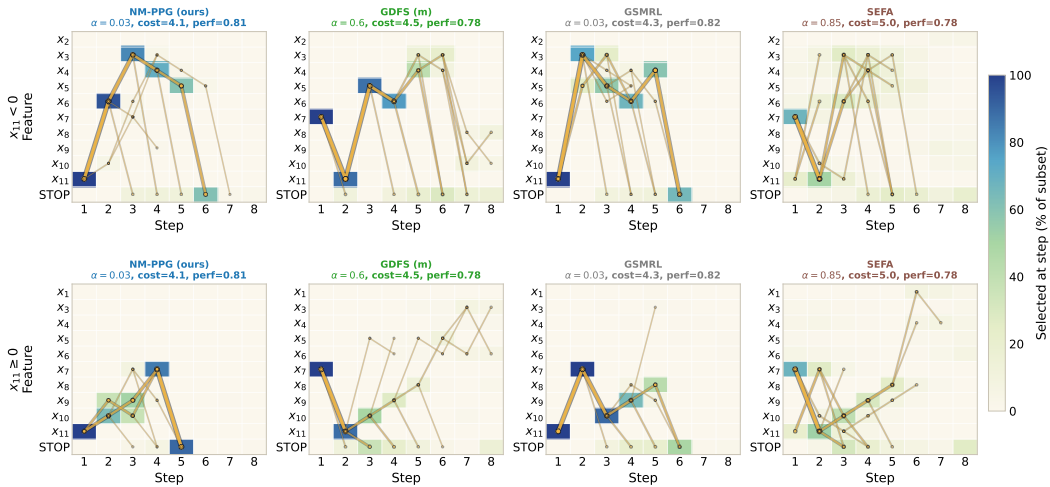


Figure 7: Acquisition trajectories on Syn3. Rows show instances with $x_{11} < 0$ and instances with $x_{11} \geq 0$. NM-PPG is compared with GDFS, GSMRL, and SEFA using feature-by-step acquisition-frequency heatmaps.

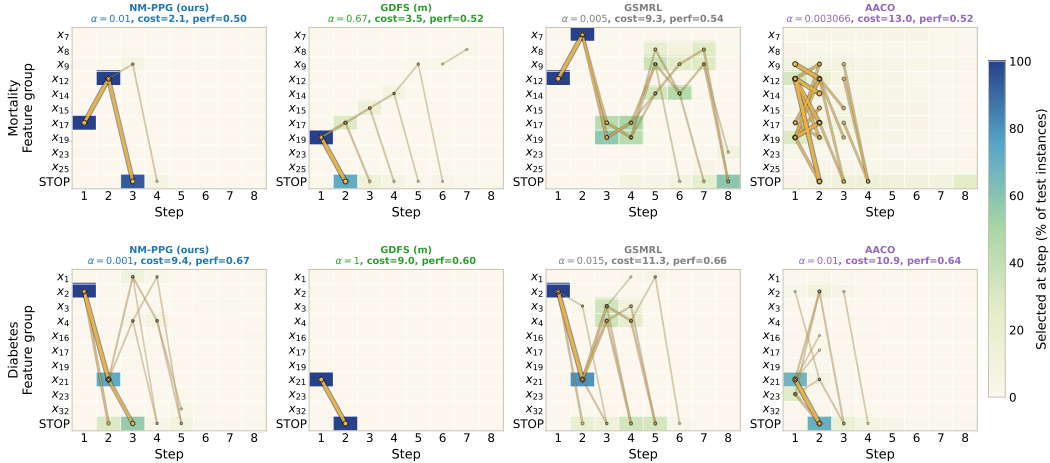


Figure 8: Acquisition trajectories on NHANES Mortality and NHANES Diabetes. NM-PPG is compared with GDFS, GSMRL, and AACO using feature-by-step acquisition-frequency heatmaps.

C.6 Runtime

Tables 3 and 4 report the training and evaluation runtime for each method and dataset, excluding shared pretraining time.

Table 3 shows that NM-PPG has training runtime that is close to the myopic methods, although it is larger overall because it optimizes a non-myopic rollout rather than a one-step acquisition rule. This additional cost is moderate relative to the gain in expressivity: NM-PPG can identify non-myopic structure while remaining comparable in runtime to RL-based non-myopic methods such as GSMRL and OL. AACO and SEFA, which are also non-myopic, are often cheaper to train, but they do not optimize the full AFA-POMDP in the same sense as NM-PPG and RL methods. Instead, they use approximations tailored to the AFA structure, exploiting that non-myopic feature acquisition requires reasoning about jointly informative feature sets. Their weaker overall performance indicates that these approximations do not fully capture long-term cost minimization in the underlying POMDP.

Table 4 shows that NM-PPG is very fast at evaluation time, with runtime similar to the other learned policies. This is important because deployment only requires a forward pass of the policy and predictor along the acquired feature path. AACO is non-parametric and does not train a separate acquisition policy, but under our protocol it still performs training-data rollouts for predictor alignment; its nearest-neighbor and candidate-subset computations also explain the larger evaluation runtime in Table 4.

C.7 Training Dynamics

Figure 9 shows representative training dynamics for NM-PPG on the same datasets as Figure 1. Each row corresponds to one dataset and one value of the trade-off parameter α , while the columns show prediction loss, acquisition cost, and the full cost-loss objective. Each panel contains both training and validation curves. The validation objective is the value of (2) evaluated on the validation split with the deterministic policy, while the training objective is the analogous quantity computed on the training rollout. For readability, each curve is shown as a moving average of the per-epoch values saved during training. Dashed vertical lines indicate transitions between the staged values of τ_{soft} used in Alg. 1, and the solid black line marks the epoch selected by validation model selection.

The curves show that NM-PPG does not simply improve prediction by acquiring all features. Instead, prediction loss, acquisition cost, and the combined objective evolve jointly on both the training and validation splits. The stage transitions also show that the optimization remains stable as τ_{soft} is annealed, which supports the staged training procedure in Alg. 1. This is useful in practice because it avoids tuning a dataset-specific temperature schedule while still allowing the relaxed policy to become increasingly close to the discrete deployment policy.

Table 3: Training runtime in seconds for each dataset and method. Values are averaged across values of α and seeds. A dash indicates that the method is unsupported for the dataset or that no measured runtime is available.

Dataset	NM-PPG	DiFA (m)	DIME (m)	GDFS (m)	AACO	SEFA	GSMRL	OL
Cube-NM ($n_c = 5, \sigma = 0.1$)	3328	426	466	1288	4123	1491	3876	1146
Cube-NM ($n_c = 5, \sigma = 0.2$)	3337	428	450	515	2604	1483	6751	813
Syn1	7583	5587	3473	5499	7616	2594	15616	5061
Syn3	8624	3262	2671	2864	8691	2778	13766	5740
Connect4	6875	2520	2367	3041	18000	5302	18000	3083
Splice	1246	306	271	294	1190	762	766	758
EngineFaultDB	7663	1250	2319	2667	4806	1979	7344	1184
Metabric	1214	267	182	225	1028	1167	1437	326
Mortality	3084	528	443	524	2910	1274	5326	763
Diabetes	10286	2277	1796	2151	7579	4896	7726	6038
MNIST	11334	7803	8011	9776	–	–	18000	12451
Fashion-MNIST	10499	9062	8091	10084	–	–	15387	12512

Table 4: Evaluation runtime in seconds for each dataset and method. Values are averaged across values of α and seeds. A dash indicates that the method is unsupported for the dataset.

Dataset	NM-PPG	DiFA (m)	DIME (m)	GDFS (m)	AACO	SEFA	GSMRL	OL
Cube-NM ($n_c = 5, \sigma = 0.1$)	12.6	9.1	10.4	10.3	241	159	17.9	8.7
Cube-NM ($n_c = 5, \sigma = 0.2$)	15.3	9.2	9.3	10.1	166	130	19.5	9.7
Syn1	44.2	38.8	31.1	31.9	333	316	55.0	78.1
Syn3	59.9	35.9	35.9	30.7	371	281	59.1	77.4
Connect4	92.3	67.3	62.1	78.3	1653	460	110	105
Splice	2.1	2.1	1.8	2.0	53.6	15.8	3.7	2.4
EngineFaultDB	22.6	17.6	16.6	18.6	260	133	38.3	12.4
Metabric	2.7	2.6	2.1	3.0	63.9	106	3.2	2.3
Mortality	13.0	8.1	7.3	7.8	146	74.9	19.1	3.3
Diabetes	38.7	31.2	28.9	30.4	398	211	65.3	35.8
MNIST	98.2	93.3	79.6	88.7	–	–	174	69.1
Fashion-MNIST	86.9	83.3	65.4	78.7	–	–	120	73.6

C.8 Method-Group Result Grids

Figures 10 and 11 provide larger versions of the main result grid, separated by baseline class. Figure 10 compares NM-PPG with the myopic baselines, while Figure 11 compares NM-PPG with the non-myopic baselines. Both figures use the same datasets, metrics, and styling as Figure 1.

D Additional Details on the Continuous Relaxation

We briefly clarify several aspects of the relaxation beyond the structural claims in Theorem 2. First, the relaxed sample $\tilde{a}_t \in [0, 1]^{d+1}$ induces two different quantities: the relaxed stop mass $\tilde{a}_{t,d+1}$ and the conditional feature-acquisition distribution \tilde{r}_t , defined as

$$\tilde{r}_t = \text{softmax}((z_{t,1:d}/\tau_{\text{hard}} + \varepsilon_{t,1:d})/\tau_{\text{soft}}), \quad (48)$$

so \tilde{r}_t is the Gumbel-Softmax relaxation of the feature distribution conditioned on not stopping. For finite $\tau_{\text{soft}} > 0$, this is equivalent to $\tilde{r}_t = \tilde{a}_{t,1:d}/(1 - \tilde{a}_{t,d+1})$. The associated hard feature action is $r_t = \text{onehot}(\arg \max_{j \in [d]} \tilde{r}_{t,j})$, which is equivalent to sampling $r_t \sim \text{softmax}(z_{t,1:d}/\tau_{\text{hard}})$ by the Gumbel-max trick. Thus, the hard feature path is sampled conditioned on continuation, while stopping remains represented by the soft stop mass and survival weights. To see this, note that the softmax transformation and the division by $\tau_{\text{soft}} > 0$ do not change the maximizer, so

$$\arg \max_{j \in [d]} \tilde{r}_{t,j} = \arg \max_{j \in [d]} (z_{t,j}/\tau_{\text{hard}} + \varepsilon_{t,j}), \quad \mathbb{P}(r_t = e_j) = \frac{\exp(z_{t,j}/\tau_{\text{hard}})}{\sum_{\ell=1}^d \exp(z_{t,\ell}/\tau_{\text{hard}})}. \quad (49)$$

The last equality is exactly the Gumbel-max trick applied only to the feature logits $z_{t,1:d}$, which gives $r_t \sim \text{softmax}(z_{t,1:d}/\tau_{\text{hard}})$.

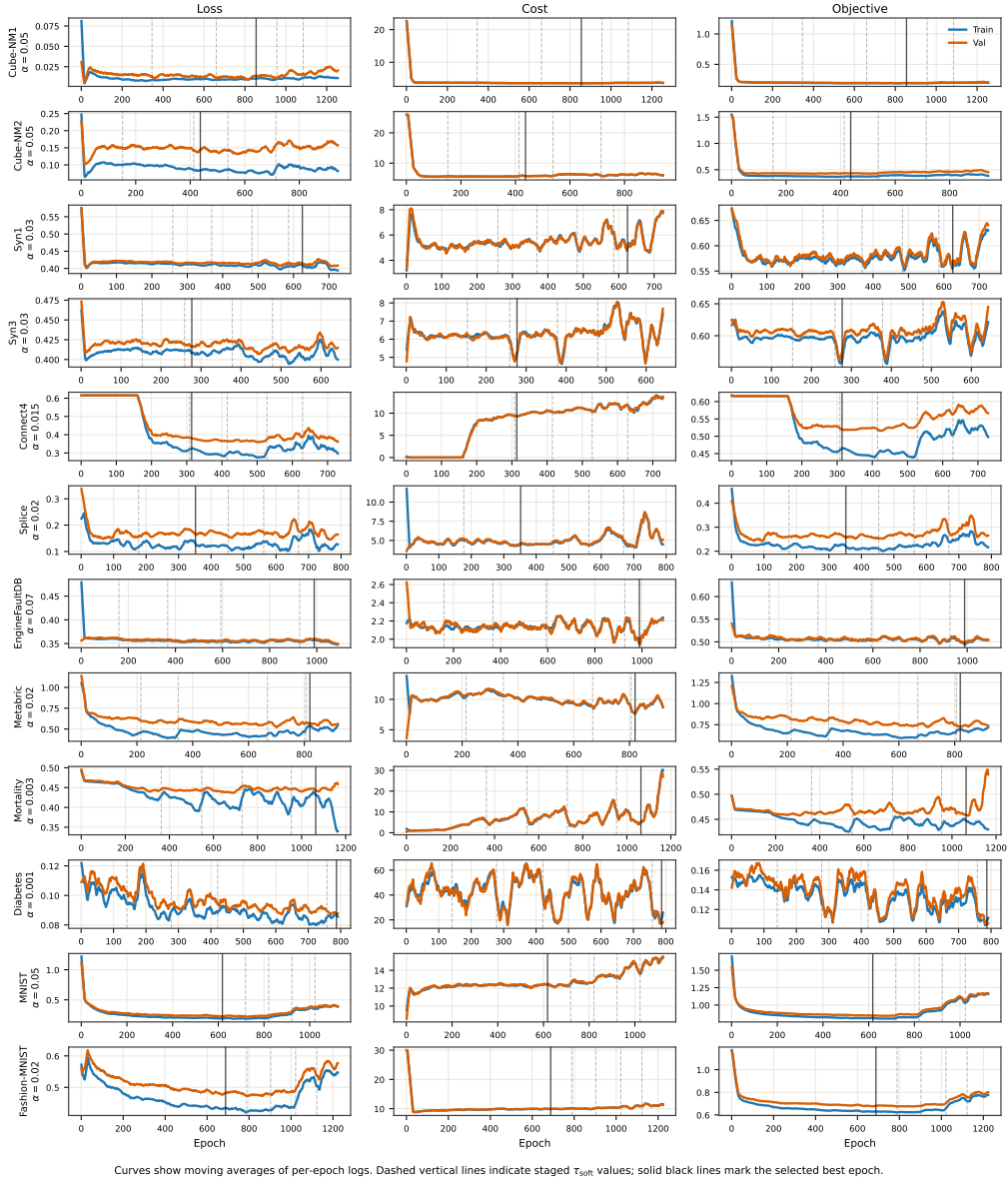


Figure 9: Training dynamics for NM-PPG. Cube-NM1 denotes Cube-NM with $n_c = 5$ and $\sigma = 0.1$, while Cube-NM2 denotes Cube-NM with $n_c = 5$ and $\sigma = 0.2$. Each row corresponds to one dataset and value of α , and columns show prediction loss, acquisition cost, and the full cost–loss objective. Blue curves show training values, orange curves show validation values, and all curves are moving averages of per-epoch logs. Dashed vertical lines indicate transitions between staged values of τ_{soft} , while solid black lines mark the epoch selected by validation model selection.

Second, the two temperatures in (4) play different roles. The parameter τ_{hard} controls the sampling distribution induced by the Gumbel perturbations: it affects both the stop-versus-continue relaxed masses in \tilde{a}_t and the conditional feature distribution from which r_t is sampled. By contrast, τ_{soft} controls the sharpness of the relaxed samples used in the differentiable computation graph. As τ_{soft} decreases, \tilde{a}_t and \tilde{r}_t become closer to one-hot vectors, so the relaxed trajectory approaches the corresponding discrete process more closely, but the resulting gradients also become sharper.

Third, feature availability is enforced by blocking logits based on the hard feature path. If $r_{t,j} = 1$, feature j is treated as acquired and its logit is set to $-\infty$ in all later steps before forming both $\tilde{a}_{t'}$ and

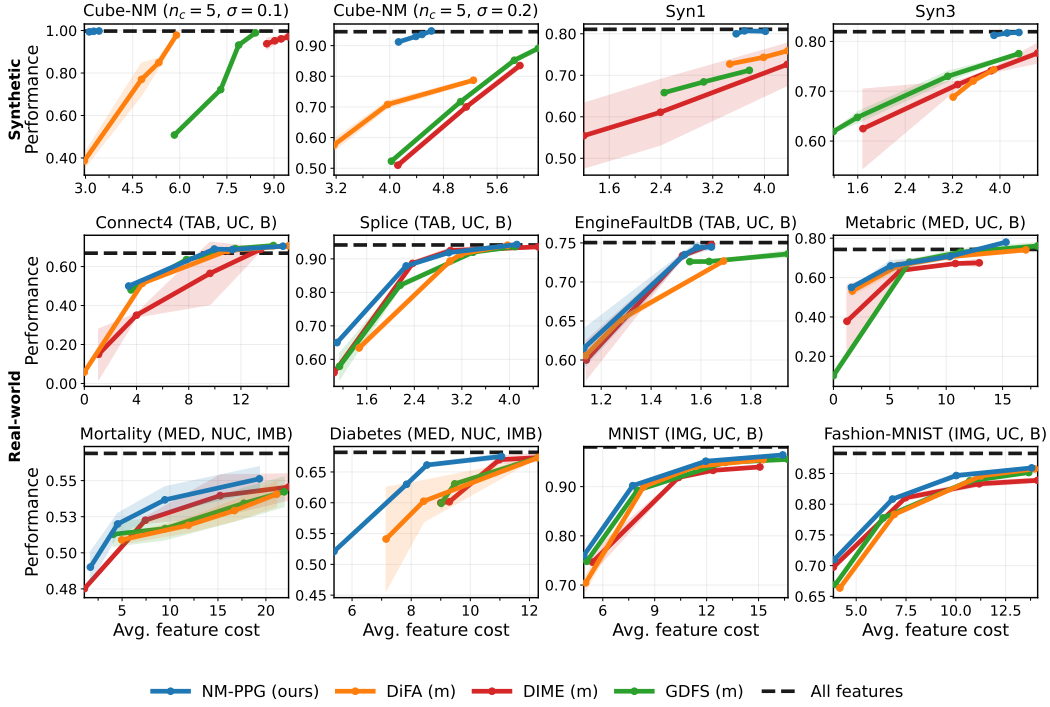


Figure 10: Results for NM-PPG, myopic baselines, and the all-features reference across synthetic (top row) and real-world (2 bottom rows) datasets. The row labels separate synthetic and real-world datasets. Performance is measured by accuracy for balanced datasets and F1-score for imbalanced datasets. The suffix (m) in the legend denotes myopic baselines. For real-world datasets, titles use the following acronyms: TAB/MED/IMG (tabular/medical/image), NUC/UC (non-uniform-cost/uniform-cost), and IMB/B (imbalanced/balanced).

r_t . This blocking is based on the hard acquisition r_t , not on whether the relaxed vector \tilde{r}_t assigns positive mass to a feature. Consequently, at every later step, \tilde{r}_t is a distribution over the feature actions that remain available after the hard acquisition prefix.

Fourth, it is important to distinguish the relaxed stop mass $\tilde{a}_{t,d+1}$ from the marginal probability of actually stopping at step t under the original discrete policy. Under an auxiliary relaxed branching interpretation for a fixed Gumbel realization, let E_t^{alive} denote the event that the relaxed trajectory is still active at step t , and let E_t^{stop} denote the event that it stops at step t . Then

$$\mathbb{P}(E_t^{\text{stop}}) = \mathbb{P}(E_t^{\text{alive}}) \mathbb{P}(\text{STOP at } t \mid E_t^{\text{alive}}). \quad (50)$$

In this auxiliary interpretation, $\mathbb{P}(E_t^{\text{alive}}) = \tilde{s}_t$ and $\mathbb{P}(\text{STOP at } t \mid E_t^{\text{alive}}) = \tilde{a}_{t,d+1}$. By unrolling the recursion in (7), we have $\tilde{s}_t = \prod_{i=0}^{t-1} (1 - \tilde{a}_{i,d+1})$ with $\tilde{s}_0 = 1$. Therefore, $\tilde{s}_t \tilde{a}_{t,d+1}$ is the relaxed stopping weight assigned to step t . These quantities are relaxed random weights, not marginal stopping probabilities under the original discrete AFA policy. This is why the terminal-loss part of (8) weights $\tilde{\ell}_t$ by $\tilde{s}_t \tilde{a}_{t,d+1}$ rather than by $\tilde{a}_{t,d+1}$ alone.

Finally, the terminal term $\tilde{s}_k \tilde{\ell}_k$ in (8) is needed to enforce the finite-horizon structure of the k -truncated relaxation. After at most k acquisition opportunities, the process must terminate. The term $\tilde{s}_k \tilde{\ell}_k$ therefore collects the remaining survival mass at step k and charges the terminal prediction loss there, ensuring that the relaxed process matches the truncated optimization problem used in training. Together, the terms $\tilde{s}_t \tilde{a}_{t,d+1}$ for $t = 0, \dots, k-1$ and the residual mass \tilde{s}_k define the full relaxed weighting over the stopping step.

The continuous relaxation enables pathwise gradients through the full truncated rollout. After reparameterization, \tilde{a}_t and \tilde{r}_t are differentiable functions of (z_t, ε_t) , and the state updates in (7) are

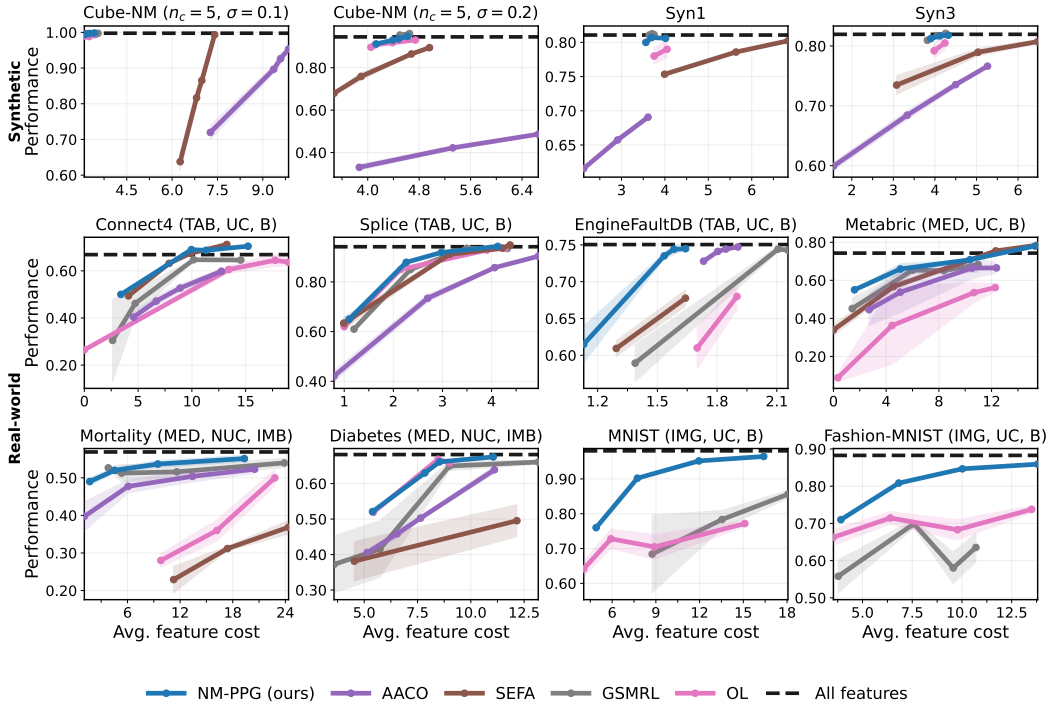


Figure 11: Results for NM-PPG, non-myopic baselines, and the all-features reference across synthetic (top row) and real-world (2 bottom rows) datasets. The row labels separate synthetic and real-world datasets. Performance is measured by accuracy for balanced datasets and F1-score for imbalanced datasets. For real-world datasets, titles use the following acronyms: TAB/MED/IMG (tabular/medical/image), NUC/UC (non-uniform-cost/uniform-cost), and IMB/B (imbalanced/balanced).

also differentiable for a fixed hard blocking pattern. Consequently, for fixed (x, y, ε) , the full k -step relaxed trajectory defines a differentiable computation graph with respect to θ . This is why the relaxed objective can be optimized by backpropagating through the entire rollout, as discussed in Section 3.2.

E Further Details on the Straight-Through Rollouts

The main benefit of the ST rollout is that it changes the *forward* optimization target so that prediction losses and feature costs are evaluated on hard masks, while retaining low-variance pathwise gradients through the soft relaxation. In a fully relaxed rollout, the predictor loss at step t is evaluated at the fractional state $x(\tilde{m}_t)$, so the policy can be updated using states that never occur at deployment. Under the ST rollout, the forward pass instead uses $\tilde{m}_t = m_t$, while the backward pass still satisfies $\partial \tilde{m}_t / \partial m_t = I$. Hence, for the loss term $\bar{\ell}_t = \ell(f_\phi(x(\tilde{m}_t)), y)$, the surrogate derivative through the mask has the form

$$\nabla_\theta^{\text{ST}} \bar{\ell}_t = \left. \frac{\partial \ell(f_\phi(x(m)), y)}{\partial m} \right|_{m=m_t} \frac{\partial \tilde{m}_t}{\partial \theta}, \quad (51)$$

where vector-Jacobian contractions are implicit. Thus, the loss derivative is evaluated at the hard mask m_t actually visited by the sampled feature path, but the gradient is propagated through the relaxed mask dynamics that produced \tilde{m}_t .

The no-stop ST rollout used by NM-PPG samples a hard feature action at every step $t < k$, conditioned on not stopping, and therefore keeps the hard feature path alive for all k acquisition steps. The purpose is to separate two sources of discreteness. For feature acquisition, we want the forward pass to use hard masks, because the predictor and policy will only see hard masks at deployment and repeated training on fractional masks can create a relaxation gap. For stopping, however, a hard sampled stop would truncate the trajectory and remove all later feature-choice gradients. We therefore keep the

stopping branch soft: the loss at step t is weighted by $\tilde{s}_t \tilde{a}_{t,d+1}$, the feature cost at step t is weighted by $\tilde{s}_t(1 - \tilde{a}_{t,d+1})$, and the forced terminal loss is weighted by \tilde{s}_k . Consequently, if the policy assigns high stop mass at an early step, later terms receive little survival mass; if it assigns low stop mass, gradients continue to shape later acquisitions. This gives feature-choice gradients at deployment-like hard states, while the stop masses receive smooth pathwise gradients that determine how much each future step should matter.

Blocking already acquired feature logits means that the step- t gradient compares the features still available after the hard acquisition prefix. Therefore, later-step gradients answer which remaining feature should be acquired next, conditional on the hard features already selected. This matches the discrete AFA constraint that a feature cannot be acquired twice, while the recursive soft dynamics still propagate the effect of earlier choices through all later masks and stopping weights.

The estimator remains biased relative to the exact gradient of the hard-forward objective, because the backward pass differentiates through a continuous relaxation rather than through the true discrete sampling process. However, compared with score-function policy gradients, it provides a lower-variance pathwise signal, and compared with a fully relaxed rollout, it evaluates the forward trajectory on hard masks that are aligned with deployment.

F AFA As a POMDP

To formalize the discussion in Section 3.1, we define the standard AFA problem in (2) as a finite-horizon, undiscounted POMDP

$$\mathcal{M} = (\mathcal{S}, \mathcal{A}, \mathcal{O}, P, O, C, \rho_0, H). \quad (52)$$

Here, \mathcal{S} is the latent state space, \mathcal{A} is the action space, \mathcal{O} is the observation space, P is the state-transition kernel, O is the observation kernel, C is the immediate cost function, ρ_0 is the initial state distribution, and H is the finite horizon, instantiated below by the truncation horizon k . We work with costs rather than rewards in order to align directly with (3).

F.1 AFA-POMDP Definition

State space. A nonterminal state at step t is

$$\omega_t = (S_t, x, y) \in 2^{[d]} \times \mathcal{X} \times \mathcal{Y}, \quad (53)$$

where $S_t \subseteq [d]$ is the set of observed feature indices, $U_t = [d] \setminus S_t$ is the set of unobserved indices, and x and y are the latent fully observed instance and label. This is equivalent to the main-text state representation (m_t, x, y) , since the binary mask m_t encodes the observed set via $m_{t,j} = \mathbf{1}\{j \in S_t\}$. We also include an absorbing terminal state ω_\perp . The initial state distribution is induced by the data distribution $p(\mathbf{x}, \mathbf{y})$ and the initial observed set,

$$\rho_0(S, x, y) = \mathbf{1}\{S = S_0\} p(\mathbf{x} = x, \mathbf{y} = y). \quad (54)$$

Throughout the paper we take $S_0 = \emptyset$, equivalently $m_0 = \mathbf{0}$. The horizon is finite because we fix a truncation horizon $k \leq d$: if the stop action has not been selected earlier, the process is forced to stop at step k .

Observations and action space. The agent does not observe (x, y) directly. Instead, at state (S_t, x, y) , it observes

$$o_t = (S_t, x_{S_t}) \in \mathcal{O}. \quad (55)$$

Thus, the observation kernel is deterministic: $O(o | S_t, x, y) = \mathbf{1}\{o = (S_t, x_{S_t})\}$. The global action set is $\mathcal{A} = \{1, \dots, d+1\}$, where actions $a \in [d]$ acquire features and $a = d+1$ is the stopping action. At state S_t , the available actions are

$$\mathcal{A}(S_t) = U_t \cup \{d+1\}, \quad (56)$$

that is, already acquired features are unavailable.

Transition dynamics. If $a \in U_t$, then $S_{t+1} = S_t \cup \{a\}$ and $\omega_{t+1} = (S_{t+1}, x, y)$. If $a = d+1$, the process terminates and transitions to ω_\perp . Although the state transition is deterministic given (x, y) , the newly revealed feature value is random from the agent’s perspective through the posterior over the unobserved components.

Belief state and observation law. After observing $o_t = (S_t, x_{S_t})$, the belief over the hidden variables is

$$b_t \triangleq (S_t, p(\mathbf{x}_{U_t}, \mathbf{y} \mid x_{S_t})). \quad (57)$$

After choosing feature $a \in U_t$, the newly observed scalar \mathbf{x}_a has predictive distribution

$$p(\mathbf{x}_a = o \mid x_{S_t}) = \mathbb{E}_{\mathbf{y} \mid x_{S_t}} [p(\mathbf{x}_a = o \mid x_{S_t}, \mathbf{y})]. \quad (58)$$

This is the probability law used in the induced belief-MDP to average over possible outcomes of acquiring feature a .

Belief update. After acquiring $a \in U_t$ and observing $\mathbf{x}_a = o$, the updated belief state is

$$b(S_t, x_{S_t}, a, o) \triangleq (S_t \cup \{a\}, p(\mathbf{x}_{U_t \setminus \{a\}}, \mathbf{y} \mid x_{S_t}, \mathbf{x}_a = o)). \quad (59)$$

Hence, the AFA-POMDP can be rewritten as a fully observable belief-MDP whose state is the posterior induced by the currently observed components (S_t, x_{S_t}) .

Immediate cost. To match the standard AFA objective in (2), we define the immediate cost for feature acquisition and stopping as

$$C((S_t, x, y), a) = \begin{cases} \alpha c(a), & a \in U_t, \\ \ell(f_\phi(x(m_t)), y), & a = d + 1. \end{cases} \quad (60)$$

For $a \in U_t$, the expected acquisition cost in belief state b_t is simply $C(b_t, a) = \alpha c(a)$. The corresponding expected stopping cost is

$$C(b_t, d + 1) = \mathbb{E}_{\mathbf{y} \mid x_{S_t}} [\ell(f_\phi(x(m_t)), \mathbf{y})]. \quad (61)$$

With forced stopping at horizon k , minimizing the expected total cost under C is equivalent to minimizing (2): the trajectory accumulates $\alpha c(a)$ for each acquired feature and pays the terminal prediction loss at the stopping mask.

Value Function and Sufficient Statistic. Given the belief-MDP above, the optimal finite-horizon value could be defined directly as a function of b_t . However, the observable pair (S_t, x_{S_t}) is a sufficient statistic for this belief state under the fixed data distribution $p(\mathbf{x}, \mathbf{y})$. Moreover, the masked representation used in the main paper,

$$x(m_t) = (m_t \odot x, m_t), \quad (62)$$

uniquely encodes (S_t, x_{S_t}) , and therefore uniquely determines the belief over unobserved components $p(\mathbf{x}_{U_t}, \mathbf{y} \mid x_{S_t})$. Thus, defining the value function with respect to $x(m_t)$ is equivalent to defining it with respect to the belief b_t . This is the form targeted in the main paper: rather than explicitly estimating the full belief over unobserved features and labels, which is generally difficult, we condition the policy and predictor directly on $x(m_t)$.

For the fixed truncation horizon k , the number of remaining acquisition opportunities at step t is $h = k - t$. We write the optimal h -step truncated cost-to-go as

$$V_h(x(m_t)) = \min \left\{ C(b_t, d + 1), \min_{a \in U_t} \left[\alpha c(a) + \mathbb{E}_{\mathbf{x}_a \mid x_{S_t}} [V_{h-1}(x(m_{t+1}))] \right] \right\}, \quad (63)$$

with $V_0(x(m_t)) = C(b_t, d + 1)$, where m_{t+1} is the mask corresponding to $S_t \cup \{a\}$ and $x(m_{t+1})$ includes the realized value x_a . The corresponding optimal h -step state-action value is

$$Q_h(x(m_t), a) \triangleq \begin{cases} C(b_t, d + 1), & a = d + 1, \\ \alpha c(a) + \mathbb{E}_{\mathbf{x}_a \mid x_{S_t}} [V_{h-1}(x(m_{t+1}))], & a \in U_t. \end{cases} \quad (64)$$

An optimal h -step policy then satisfies

$$\pi_h^*(x(m_t)) \in \arg \min_{a \in \mathcal{A}(S_t)} Q_h(x(m_t), a). \quad (65)$$

This appendix uses h -indexed value functions to make the finite-horizon Bellman recursion explicit while keeping k for the fixed truncation horizon of the overall AFA problem. Under the common initialization $S_0 = \emptyset$, equivalently $m_0 = \mathbf{0}$, we have $h = k$ at the initial state, so minimizing $J(\pi)$ in (3) over policies coincides with the optimal $h = k$ control problem characterized by (63) and (64). More generally, at step t , the relevant value is $V_{k-t}(x(m_t))$. When $k = d$, this truncated problem coincides with the full finite-horizon AFA problem.

F.2 Policy Gradient Theorem for AFA

A standard way to optimize $J(\pi_\theta)$ is via the *policy gradient theorem* [35], which expresses the gradient of the expected total cost using the score function $\nabla_\theta \log \pi_\theta(a_t | x(m_t))$. For the fixed truncation horizon k , define the policy-specific state-action value under π_θ as

$$Q^{(\pi_\theta)}(x(m_t), a) \triangleq \mathbb{E}_{\mathbf{x}_{U_t}, \mathbf{y} | x_{S_t}} \mathbb{E}_{\pi_\theta} \left[\sum_{i=t}^{t_\theta(\mathbf{x})} C((S_i, \mathbf{x}, \mathbf{y}), a_i) \mid a_t = a \right]. \quad (66)$$

Here, $t_\theta(\mathbf{x}) \leq k$ is the policy-induced stopping step in the resulting truncated trajectory, with rollout randomness left implicit. In our AFA setting, the policy gradient theorem yields

$$\nabla_\theta J(\pi_\theta) \approx \mathbb{E}_{\mathbf{x}, \mathbf{y}} \mathbb{E}_{\pi_\theta} \left[\sum_{t=0}^{t_\theta(\mathbf{x})} \hat{Q}^{(\pi_\theta)}(\mathbf{x}(m_t), a_t) \nabla_\theta \log \pi_\theta(a_t | \mathbf{x}(m_t)) \right], \quad (67)$$

where each action in the trajectory is sampled from the policy, $a_t \sim \pi_\theta(\cdot | \mathbf{x}(m_t))$. Here, $\hat{Q}^{(\pi_\theta)}$ is an approximation of the state-action value $Q^{(\pi_\theta)}$, for example via a learned critic network. This score-function form is the standard RL approach used by methods such as PPO in prior AFA work [26].

F.3 Deterministic Policy Gradient for Relaxed AFA

Section 3.2 introduces a continuous relaxation of the discrete AFA-POMDP by reparameterizing the acquisition policy with the Gumbel-Softmax construction in (4), and by defining the corresponding relaxed state dynamics and relaxed trajectory cost in (7) and (8). This yields a continuous-action control problem in which the relaxed action lies in the simplex Δ^{d+1} . Conditioned on the exogenous Gumbel noise, the relaxed policy is deterministic as a function of the current relaxed state and the parameters θ . Let $h_t \triangleq z_\theta(x(\tilde{m}_t))$ denote the policy logits at step t . We therefore define the relaxed policy map by

$$\tilde{\pi}_\theta(x(\tilde{m}_t), \varepsilon_t) \triangleq \text{softmax}((h_t / \tau_{\text{hard}} + \varepsilon_t) / \tau_{\text{soft}}), \quad \varepsilon_t \sim \text{Gumbel}(0, 1)^{d+1}. \quad (68)$$

Applying the deterministic policy gradient (DPG) theorem [37, 40, 41] to this reparameterized relaxed control problem gives

$$\nabla_\theta \tilde{J}(\theta) \approx \mathbb{E}_{\mathbf{x}, \mathbf{y}} \mathbb{E}_\varepsilon \left[\sum_{t=0}^k \nabla_\theta \tilde{\pi}_\theta(x(\tilde{m}_t), \varepsilon_t) \nabla_a \tilde{Q}^{(\pi_\theta)}(x(\tilde{m}_t), a) \Big|_{a=\tilde{\pi}_\theta(x(\tilde{m}_t), \varepsilon_t)} \right]. \quad (69)$$

Here, $\tilde{Q}^{(\pi_\theta)}$ is analogous to $\hat{Q}^{(\pi_\theta)}$ in (67), except it is defined with respect to the relaxed trajectory cost \tilde{G} in (8).

F.4 Model-Based Learning in the AFA-POMDP

The belief-MDP formulation above is conceptually useful, but solving the AFA-POMDP exactly is highly intractable. Although the horizon is at most d , the number of possible observation masks grows exponentially with d , and the belief state additionally depends on a posterior over the unobserved components of the latent state [10]. For this reason, some prior work on AFA uses an explicit belief model $p(\mathbf{x}_{U_t}, \mathbf{y} | x_{S_t})$ to reduce the search space and to support model-based acquisition decisions [10, 23, 26]. In such approaches, one uses the model over unobserved components to evaluate the expected effect of acquiring a candidate feature, rather than relying only on the currently observed input.

Following the AFA survey [10], we use the term *model-based* specifically for methods that learn or use a model of the feature-observation dynamics, i.e., a model for $p(\mathbf{x}_{U_t} | x_{S_t})$. This is the part of the belief state that determines how the AFA-POMDP evolves after a feature-acquisition action. By contrast, using a predictor $f_\phi(x(m_t))$ to approximate the label belief $p(\mathbf{y} | x_{S_t})$ does not by itself make a method model-based in this sense. Every AFA method needs such a predictive model to evaluate the terminal prediction loss after stopping: for example, the stopping cost in (60) depends on the predictor evaluated at the currently observed mask. Thus, the distinction is whether a method

models the distribution of *future observations* induced by acquiring unobserved features, not whether it contains a supervised predictor for the label. Under this terminology, NM-PPG is model-free: it learns a policy and predictor from observed training rollouts, but does not learn or query a model for $p(\mathbf{x}_{U_t} | x_{S_t})$.

Modeling $p(\mathbf{x}_{U_t} | x_{S_t})$ is essentially an imputation problem from the missing-feature literature [19, 57], and is itself a highly intractable problem in general. In principle, combining the policy with a model for $p(\mathbf{x}_{U_t} | x_{S_t})$, together with the induced label belief $p(\mathbf{y} | x_{S_t})$, yields a model-based approximation to the belief state $p(\mathbf{x}_{U_t}, \mathbf{y} | x_{S_t})$. Several AFA methods pursue this idea using *deep arbitrary conditional generative models* [19, 23, 26]. However, accurately learning this belief over unobserved features is itself difficult, and these generative models are known to be unstable and often hard to train in practice [12, 31]. As a result, when the imputation model is inaccurate, it can even reduce performance, depending on the complexity of the dataset. This is one reason why the main paper instead emphasizes direct conditioning on the sufficient statistic $x(m_t)$, rather than requiring an explicit, high-quality model for the full belief over unobserved components.

G Myopic vs. Non-Myopic Policies in AFA

A *myopic* policy in the AFA-POMDP is a policy that optimizes the 1-step truncated value function. Specializing (63) and (64) to $h = 1$, the myopic cost-to-go is

$$V_1(x(m_t)) = \min_{a \in \mathcal{A}(S_t)} Q_1(x(m_t), a), \quad (70)$$

where the one-step state-action value is

$$Q_1(x(m_t), a) \triangleq \begin{cases} C(b_t, d+1), & a = d+1, \\ \alpha c(a) + \mathbb{E}_{\mathbf{x}_a | x_{S_t}} [V_0(x(m_{t+1}))], & a \in U_t. \end{cases} \quad (71)$$

The base case in (71) is $V_0(x(m_{t+1})) \triangleq C(b_{t+1}, d+1)$, i.e., with zero acquisition steps remaining after observing the next mask m_{t+1} , the only available operation is to stop and incur the expected stopping cost. The corresponding myopic policy is therefore

$$\pi_1^*(x(m_t)) \in \arg \min_{a \in \mathcal{A}(S_t)} Q_1(x(m_t), a). \quad (72)$$

Intuitively, a myopic policy asks: *if we either stop now or acquire one more feature and then stop, which action gives the lowest expected total cost?* By contrast, a *non-myopic* policy plans with V_h for $h > 1$. At step t , the k -truncated AFA problem studied in this paper corresponds to V_{k-t} , while the full untruncated AFA problem is recovered when $k = d$. Thus, non-myopic selection accounts for how the current acquisition changes future acquisition opportunities and the eventual stopping decision [10].

The benefit of non-myopic selection is highly dataset dependent. If the predictive utility of the remaining features is largely additive, if the best next acquisition does not depend strongly on future observations, and if feature costs are nearly uniform, then repeated myopic selection is often close to, or even exactly, optimal. This helps explain why recent AFA benchmarks frequently find strong myopic baselines on many datasets, while datasets that are explicitly constructed to require long-term planning favor non-myopic methods [10, 31]. Non-myopic selection becomes important precisely when the value of an acquisition cannot be assessed from its immediate one-step effect alone.

Three situations are especially important. First, non-myopic planning is needed when features are *jointly informative* but only weakly informative marginally. In that case, a feature may appear unhelpful under the 1-step objective in (71), even though it is valuable because it enables a later feature whose usefulness only appears after the first one has been observed. Second, non-myopic planning is crucial when there are *context features*: a feature that is itself weakly informative about the label, but indicates which other feature is informative for the current instance. This is the setting in which AFA most clearly benefits from being both *non-myopic* and *adaptive*, since the first acquisition is useful not because it directly predicts the label, but because it routes different instances toward different later acquisitions. In such problems, the best feature to acquire next varies across instances, and this variation only becomes visible after observing the context feature. Third, non-myopic planning becomes especially important under *non-uniform feature costs*. A cheap feature may have little immediate predictive value, yet still be optimal because it reveals whether a more expensive

acquisition is necessary at all. A myopic rule can therefore prefer an immediately informative but consistently costly feature, while a non-myopic rule can exploit a cheaper multi-step path with lower total expected cost.

Taken together, these observations clarify why no universal advantage of non-myopic AFA should be expected across all datasets. The value of non-myopic planning depends on the extent to which long-term feature interactions, context-dependent routing, and heterogeneous acquisition costs shape the decision problem. When these effects are weak, myopic policies can be highly competitive. When they are strong, non-myopic and adaptive selection becomes essential.